Petroleum Science 23 (2026) 1842–1859

Contents lists available at ScienceDirect

Petroleum Science

journal homepage: www.keaipublishing.com/en/journals/petroleum-science

Original Paper

A novel local maximum synchrosqueezing W transform for reservoir characterization

Chao-He Wang [a], Zhao-Yun Zong [a,*], Xing-Yao Yin [a], Kun Li [b], Ying-Hao Zuo [a]

[a] State Key Laboratory of Deep Oil and Gas, China University of Petroleum (East China), Qingdao, 266580, Shandong, China
[b] College of Computer Science and Technology, China University of Petroleum (East China), Qingdao, 266580, Shandong, China

ARTICLE INFO

Article history:
Received 29 March 2025
Received in revised form
29 September 2025
Accepted 18 November 2025
Available online 21 November 2025

Edited by Meng-Jiao Zhou

Keywords:
Reservoir characterization
W transform (WT)
Time-frequency analysis (TFA)
Local maximum synchrosqueezing transform (LMSST)

ABSTRACT

Time-frequency analysis (TFA) serves as a critical tool in seismic signal processing and interpretation, particularly for characterizing non-stationary signals. However, conventional TFA methods, such as the short-time Fourier transform (STFT) and continuous wavelet transform (CWT), suffer from inherent limitations, including energy smearing and insufficient time-frequency resolution, which hinder their ability to meet the demands of high-precision seismic interpretation. By detecting local maxima along the frequency direction, LMSST significantly improves energy concentration in time-frequency representations (TFRs). Meanwhile, the W transform is known for high resolution in low-frequency regions and a flexible windowing function, which surpasses conventional TFA methods. However, both methods face limitations when applied independently to complex seismic signals, particularly in scenarios demanding high precision and resolution. To overcome these challenges, the local maximum synchrosqueezing W transform (LMSSWT) is proposed. This approach combines the adaptive windowing of the W transform with the precise frequency reallocation of the LMSST, resulting in a more centralized and energy-concentrated time-frequency representation. Furthermore, an inverse LMSSWT is also derived to ensure completeness and accurate signal reconstruction. By synergizing the W transform's adaptive windowing with the energy concentration of LMSST, LMSSWT overcomes key limitations in time-frequency analysis of complex seismic signals, offering a powerful tool for high-resolution reservoir prediction and hydrocarbon detection. The effectiveness and applicability of the proposed method are validated through synthetic tests and practical data applications.

1. Introduction

Signal analysis is widely applied in the fields of seismic processing and interpretation (Huang et al., 2024; Lan et al., 2022; Zhang et al., 2024; Zong et al., 2023; Zhang et al., 2024; Zong et al., 2025). Time frequency analysis (TFA) is a key technique in this context, enabling the transformation of one-dimensional time series into a two-dimensional time-frequency (TF) plane (Huang et al., 2016; Wang and Lu, 2018; Liu et al., 2023a,b). This 2D representation captures temporal fluctuations in signal properties, crucial for understanding the complexities of geological formations. Linear TFA methods, such as short-time Fourier transform (STFT) (Gabor, 1946), continuous wavelet transform (CWT) (Daubechies and Bates, 1993; Li et al., 2024; Sinha et al., 2003), and S transform (ST) (Kakhki et al., 2022; Liu et al., 2024; Stockwell et al., 1996), have provided approximate localized signal characteristics, offering an advantage over traditional Fourier transforms, which are limited to global signal information. However, these conventional techniques are constrained by the Heisenberg uncertainty principle. Consequently, these representations are often blurred and have fallen short of accurately capturing the intricacies of time-varying signals.

To enhance the readability and precision of these TF representations, reassignment methods (RM) were introduced as post-processing tools for classical TFA techniques (Auger and Flandrin, 1995). RM enhances sharpness in the TF plane by recalculating the position of each TF point based on phase information, followed by a 2D reassignment integral. This process yields a clearer TF visualization. However, it relies on absolute TF representations, which prevents the reconstruction of the original signal. To address this limitation, the synchrosqueezing transform (SST) was

* Corresponding author.
E-mail address: zongzhaoyun@upc.edu.cn (Z.-Y. Zong).
Peer review under the responsibility of China University of Petroleum (Beijing).

https://doi.org/10.1016/j.petsci.2025.11.034

developed. SST overcomes the issue by compressing information along the frequency axis, enabling signal reconstruction. The initial SST was created from CWT (Daubechies et al., 2011), and later, the synchronous compression transformation based on STFT was improved (Meignen et al., 2019). Notably, when applied to strongly frequency-modulated signals, SST tends to produce smeared TF energy representations, which can obscure critical details in seismic and geological data interpretation.

To overcome the problem, several concentrated SST methods have been developed, aiming to achieve ideal TFA (ITFA), which encompasses high TF resolution, perfect reconstruction capability, and computational efficiency. Methods such as demodulation SST (Cao et al., 2016), statistical SST (Chen et al., 2023), time sparse ST (TSST) (Chen et al., 2024) and local maximum SST (LMSST) (Yu et al., 2019) have been, effectively applied in the sedimentary cycle division (Tian et al., 2022), seismic attenuation estimation (Liu et al., 2022; Xue et al., 2021), seismic interpretation (Li et al., 2020; Song et al., 2023, 2024), seismic ground roll suppression (Lin et al., 2022) and random noise attenuation (Anvari et al., 2017). Among them, LMSST achieves highly accurate instantaneous frequency (IF) estimation, which significantly improves energy concentration. However, LMSST struggles to represent the amplitude of strongly time-varying signals, making it challenging to obtain precise TF information for signals with intense FM. The local maximum synchrosqueezing Chirplet transform (LMSSCT) was thus proposed to complement LMSST for strongly nonstationary signals (He et al., 2021). Despite these advancements, none of these methods can handle nonstationary signals flexibly, primarily due to limitations imposed by fixed window function lengths.

Recently, Wang (2021) introduced the W-Transform (WT) by modifying the Gaussian window function in ST, using a time-dependent dominant frequency. WT aims to center spectral energy around the dominant frequency of a waveform, thus achieving superior low-frequency time resolution (Luo et al., 2022). Subsequent enhancements to the WT have focused on two main aspects. The first involves modifying the window function itself, exemplified by the three-parameter WT (Chen et al., 2022), generalized WT (GWT) (Li et al., 2022), linear canonical WT (LCWT) (Zhao et al., 2024b), and the fractional-order W-Transform (FrWT) (Zhao et al., 2024a), and the normalized W Transform (Chen et al., 2025), which adjusts window function parameters to prevent energy split around the instantaneous frequency. Nonetheless, these modifications have a limited impact on improving energy concentration and still exhibit energy divergence at frequencies far from the instantaneous frequency. The second approach combines the WT with other TFAs, such as WT with a chirp-modulated window (Zhao et al., 2023) and the window parameter-optimized WT (Wu et al., 2024), aiming to leverage the strengths of multiple methods to enhance energy concentration. Despite these improvements, the computational demand of the WT, especially when combined with other methods, significantly increases, posing a challenge for large-scale applications in seismic data processing. In addition, since WT is proposed based on STFT, the TF post-processing also applies to the results obtained by WT. To improve the TF resolution of WT, the synchro extracting algorithm based on WT (SEWT) is proposed (Luo and Zong, 2023), which has been proven to be equivalent to ideal TFA for weakly time-varying signals. One drawback is that the TFR provided by the SEWT is still heavily blurry when addressing strongly time-varying and nonstationary seismic signals.

In this paper, a novel method combining LMSST and WT, termed LMSSWT, is proposed for reservoir characterization. First, based on a theoretical analysis of the performance of WT in nonstationary seismic signals, two new post-processing transforms, SSWT and LMSSWT methods are derived to lay a theoretical foundation for improving the accuracy of signal analysis. Secondly, the superior performance of the proposed method in intermediate frequency detection, mode decomposition and reconstruction, and noise resistance is verified through tests on numerical signals. Then, by applying the geological model and actual seismic profiles and comparing them with traditional seismic analysis methods. Obviously, the proposed method can more accurately characterize the top and bottom boundaries of the sand body. Finally, the innovative method is applied to further achieve 3D characterization of channel boundaries and reservoir description. The results effectively demonstrate the efficacy and reliability of the method. The main contributions of this research are as follows.

(1) We propose novel time-frequency analysis methods, SSWT and LMSSWT, which are equipped with a more flexible window function and greater frequency-reassignment operators.
(2) The superior performance of the proposed method in IF detection, mode decomposition, and reconstruction, and noise resistance is verified. Meanwhile, traditional seismic analysis methods and variants are compared.
(3) This method is applied to geological models and seismic profiles for thin layer recognition. The boundary characterization of a 3D channel reservoir is clearer after being processed by the method.

2. Method

To overcome the problem of limited window functions and improve the precision of the TF representations, two novel post-processing analyses, SSWT and LMSSWT are derived based on the W transform, which has a flexible window function and shows high time resolution at low frequencies (Wang, 2021).

A multi-component signal with amplitude-modulated (AM) and frequency-modulated (FM) laws can be modelled as:

$$s(t)=\sum_{k=1}^{n}A_k(t)\mathrm{e}^{\mathrm{i}\varphi_k(t)} \tag{1}$$

where $A_k(t)$ is the instantaneous amplitude (IA), t is the time, and $\varphi_k(t)$ denotes the instantaneous phase.

The eventual developed goal of the TFA method is to achieve the ideal TFA, which can be expressed as:

$$\mathrm{ITFA}(t,f)=\sum_{k=1}^{n}A_k(t)\mathrm{e}^{\mathrm{i}\varphi_k(t)}\delta\left(f-\varphi_k'(t)\right) \tag{2}$$

where k is the number of multiple components, and δ is the Dirac function. $A_k(t)$ are the instantaneous amplitude (IA). $\varphi_k(t)$ denotes the instantaneous phase, and its one-order derivative $\varphi_k{}'(t)$ is the instantaneous frequency (IF).

When this signal is presented in the TF domain, the STFT of the function $s\in L^2(\mathbb{R})$ using a real and even window $g\in L^2(\mathbb{R})$ is written as:

$$G(t,f)=\int_{-\infty}^{\infty}g(u-t)s(u)\mathrm{e}^{-\mathrm{i}f(u-t)}\mathrm{d}u \tag{3}$$

where $|G(t,f)|$ is defined as the spectrogram of STFT. The STFT enables the expansion of one-dimensional (1D) time-series signals into a two-dimensional (2D) time-frequency (TF) plane, thereby facilitating the effective extraction of instantaneous amplitude (IA) and instantaneous frequency (IF) information inherent to the signal. Beyond this capability, another pivotal application of the STFT lies in its ability to reconstruct individual mono-component modes from a multi-component signal.

To fully leverage the advantage of the W transform's high resolution in the low-frequency band and to avoid the frequency splitting phenomenon at the dominant frequency. We use the three-parameter W transform (TPWT) (Chen et al., 2022; Liu et al., 2024) as the default W transform algorithm. As an improved algorithm of the original W transform, the TRWT method suppresses the amplitude splitting artifact exhibited by the WT at the dominant frequency, resulting in a concentration of the time-frequency spectrum's energy around the main frequency. This enhancement facilitates the precise analysis of energy distribution through a subsequent post-processing algorithm. The main difference between TRWT and the above STFT is the Gaussian window, which is defined as:

$$g_w(u,f;t)=\frac{1}{\sqrt{2\pi}\sigma(t,f;k_1,k_2,p)}\mathrm{e}^{-\frac{u^2}{2\sigma^2(t,f;k_1,k_2,p)}} \tag{4}$$

where the parameter σ is defined as:

$$\sigma(t,f;k_1,k_2,p)=\frac{1}{\sqrt[p]{\left[\frac{f_0(t)}{k_1}\right]^p+\left[\frac{|f_0(t)-f|}{k_2}\right]^p}} \tag{5}$$

where the $f_0(t)$ is the instantaneous frequency at the time t.The three parameters k_1, k_2 and p control the shape of the Gaussian window. Benefiting from these parameters, TPWT produces a more highly-focused energy distribution in the time-frequency spectrum. We use TPWT as the default WT method. And the expression of WT is as follows:

$$\begin{aligned}W(t,f)&=\int_{-\infty}^{\infty}g_w(u-t)s(u)\mathrm{e}^{-if(u-t)}\mathrm{d}u\\&=\int_{-\infty}^{+\infty}\frac{\sqrt[p]{\left[\frac{f_0(t)}{k_1}\right]^p+\left[\frac{|f_0(t)-f|}{k_2}\right]^p}}{\sqrt{2\pi}}\mathrm{e}^{-\frac{(u-t)^2}{2k^2}\left[\sqrt[p]{\left[\frac{f_0(t)}{k_1}\right]^p+\left[\frac{|f_0(t)-f|}{k_2}\right]^p}\right]^2}\\&\qquad s(u)\mathrm{e}^{-if(u-t)}\mathrm{d}u\end{aligned} \tag{6}$$

For Eq. (3), we first perform integration with respect to the frequency variable, yielding the following result:

$$\begin{aligned}\int_{-\infty}^{+\infty}G(t,f)\mathrm{d}f&=\int_{-\infty}^{+\infty}\int_{-\infty}^{\infty}g(u-t)s(u)\mathrm{e}^{-if(u-t)}\mathrm{d}u\mathrm{d}f\\&=2\pi\int_{-\infty}^{+\infty}g(u-t)s(u)\delta(u-t)\mathrm{d}u\\&=2\pi g(0)s(t)\end{aligned} \tag{7}$$

Therefore, the original signal $s(t)$ can be recovered by

$$s(t)=(2\pi g(0))^{-1}\int_{-\infty}^{+\infty}G(t,f)\mathrm{d}f \tag{8}$$

To further explore the STFT result of the signal given by Eq. (1), it is necessary to assume that the analyzed signal is a weakly frequency-varying signal. when $\exists\varepsilon$ is sufficiently small, $|A_k'(t)|\le\varepsilon\left|\varphi_k''(t)\right|\le\varepsilon$ for $\forall t$.The first-order expansion around $u=t$ of the signal in the form is derived as:

$$s(u)=\sum_{k=1}^{K}A_k(t)\mathrm{e}^{i\left(\varphi_k(t)+\varphi_k'(t)(u-t)\right)} \tag{9}$$

where $A_k(u)=A_k(t)$, and $\varphi_k(u)=\varphi_k(t)+\varphi_k'(t)(u-t)$, the higher-order terms are neglected.

Substituting Eq. (9) into Eq. (3), it can be obtained:

$$\begin{aligned}G(t,f)&=\int_{-\infty}^{+\infty}g(u-t)\sum_{k=1}^{K}A_k(t)\mathrm{e}^{i\left(\varphi_k(t)+\varphi_k'(t)(u-t)\right)}\mathrm{e}^{-if(u-t)}\mathrm{d}u\\&=\sum_{k=1}^{K}A_k(t)\mathrm{e}^{i\varphi_k(t)}\int_{-\infty}^{+\infty}\mathrm{e}^{i\left(\varphi_k'(t)(u-t)-f(u-t)\right)}g(u-t)\mathrm{d}(u-t)u\\&=\sum_{k=1}^{K}A_k(t)\mathrm{e}^{i\varphi_k(t)}\widehat{g}\left(f-\varphi_k'(t)\right)\end{aligned} \tag{10}$$

where $\widehat{\mathrm{g}}$ denotes the Fourier transform of the window and $\mathrm{supp}(\widehat{g})\in[-\Delta,\Delta]$.When each mode is well-separated within the time-frequency (TF) plane, distinct components occupy discrete TF domains. Consequently, each component can be reconstructed by integrating the TF coefficients $G(t,f)$ around their respective IF $\varphi_k'(t)$ in frequency direction as:

$$s_k(t)=(2\pi g(0))^{-1}\int_{|f-\varphi_k'(t)|\le\Delta}\int G(t,f)\mathrm{d}f \tag{11}$$

Eq. (8) illustrates that, for the STFT-based post-processing reassignment technique, the way to possess the ability of signal reconstruction is to consider only frequency reassignment. To observe the time-varying TF features more precisely, the SST technique is designed to improve the readability of TF representation (Daubechies et al., 2011). The SST expression is written as:

$$\mathrm{SST}(t,\eta)=\int_{-\infty}^{+\infty}G(t,f)\delta(\eta-f_0(t,f))\mathrm{d}f \tag{12}$$

Then the SST is applied to squeeze the TF coefficient $W(\tau,f)$ of the W transform on the instantaneous frequency trajectory. According to Eq. (10), the resulting SST expression is defined as SSWT. And Synchrosqueezing W transform (SSWT) expression can be expressed as follows:

$$\mathrm{SSWT}(t,\eta)=\mathrm{SST}(W(t,\eta))=\int_{-\infty}^{+\infty}W(t,f)\delta(\eta-f_0(t,f))\mathrm{d}f \tag{13}$$

where

$$f_0(t,f)=\frac{\partial_t W(t,f)}{iW(t,f)} \tag{14}$$

Furthermore, the $\partial_t W(t,f)$ can also be calculated as:

$$\begin{aligned}\partial_t W(t,f)&=\partial_t\left(\int_{-\infty}^{+\infty}g_{\mathrm{w}}(u-t)s(u)\mathrm{e}^{-if(u-t)}\mathrm{d}u\right)\\&=-\int_{-\infty}^{+\infty}g_{\mathrm{w}}{}'(u-t)s(u)\mathrm{e}^{-if(u-t)}\mathrm{d}u+if\int_{-\infty}^{+\infty}g_{\mathrm{w}}(u-t)s(u)\\&\mathrm{e}^{-if(u-t)}\mathrm{d}u=-W^{g_{\mathrm{w}}'}(t,f)+ifW(t,f)\end{aligned} \tag{15}$$

Such that the $f_0(t,f)$ can be rewritten as:

$$f_0(t,f)=f+i\frac{W^{g_{\mathrm{w}}'}(t,f)}{W(t,f)} \tag{16}$$

In practical calculations, the real part of $f_0(t,f)$ is required as:

$$f_0(t,f)=f-\mathrm{Im}\left(\frac{W^{g_{\mathrm{w}}'}(t,f)}{W(t,f)}\right) \tag{17}$$

Substitute Eq. (4) into Eq. (3), and the results of SSWT transformation can be obtained by setting the integral term and squeezing the dispersed time-frequency energy:

$$\begin{aligned}\int_{-\infty}^{+\infty}\mathrm{SSWT}(t,\eta)\mathrm{d}\eta&=\int_{-\infty}^{+\infty}\int_{-\infty}^{+\infty}W(t,f)\delta(\eta-f_0(t,f))\mathrm{d}f\mathrm{d}\eta\\&=\int_{-\infty}^{+\infty}W(t,f)\int_{-\infty}^{+\infty}\delta(\eta-f_0(t,f))\mathrm{d}f\mathrm{d}\eta=\int_{-\infty}^{+\infty}\int_{-\infty}^{+\infty}\frac{\sqrt[p]{\left[\frac{f_0(t)}{k_1}\right]^p+\left[\frac{|f_0(t)-f|}{k_2}\right]^p}}{\sqrt{2\pi}}\mathrm{e}^{-\frac{(u-t)^2}{2k^2}\left[\sqrt[p]{\left[\frac{f_0(t)}{k_1}\right]^p+\left[\frac{|f_0(t)-f|}{k_2}\right]^p}\right]^2}s(u)\mathrm{e}^{-\mathrm{i}f(u-t)}\mathrm{d}u\mathrm{d}f\\&=\int_{-\infty}^{+\infty}\int_{-\infty}^{+\infty}g_{\mathrm{w}}(u-t)s(u)\mathrm{e}^{-\mathrm{i}f(u-t)}\mathrm{d}u\mathrm{d}f=2\pi\int_{-\infty}^{+\infty}g_{\mathrm{w}}(u-t)s(u)\delta(u-t)\mathrm{d}u=2\pi g_{\mathrm{w}}(0)s(t)\end{aligned}\tag{18}$$

SST is a technique that only considers frequency reassignment. According to Eq. (8), SSWT can reconstruct the signal by integrating the TF coefficients $W(t,f)$ around their IF $\varphi_k'(t)$ in the frequency direction. The signal $s(t)$ can be reconstructed using an expression similar to Eq. (11) as:

$$s_k(t)=(2\pi g_{\mathrm{w}}(0))^{-1}\int_{|f-\varphi_k'(t)|\leqslant d_s}\mathrm{SSWT}(t,f)\mathrm{d}f\tag{19}$$

where d_s denotes the reconstruction bandwidth of SSWT. Due to the ability of signal reconstruction, the SSWT can be used in applications of signal de-noising, data compression, and mono-component mode decomposition. Ideally, all smeared time-frequency coefficients should be reassigned to the instantaneous frequency (IF) trajectories along the frequency direction, thereby enabling simultaneous acquisition of the ITFA representation and preservation of signal reconstruction capability. As indicated in Eq. (10), the spectrogram is concentrated along the IF trajectories but exhibits a smeared energy distribution, which can be expressed as:

$$|W(t,f)|=\sum_{k=1}^{n}A_k(t)\widehat{g}_{\mathrm{w}}(f-\varphi_k'(t))\tag{20}$$

Based on the analysis, the only post-processing method that retains the capacity for mode recovery in time-frequency (TF) analysis is reassigning the TF coefficients in the frequency direction. Thus, a technique known as LMSST (Chen et al., 2024) is expressed as:

$$\mathrm{LMSST}(t,\eta)=\int_{-\infty}^{+\infty}G(t,f)\delta(\eta-f_m(t,f))\mathrm{d}f\tag{21}$$

To observe the time-varying TF features more precisely, LMSST is proposed to gather the diffused TF energy by a novel frequency RM operator. The expression of the operator can be written as:

$$f_m(t,f)=\begin{cases}\underset{f}{\mathrm{argmax}}|W(t,f)|,f\in[f-\Delta,f+\Delta], & \text{if } |W(t,f)|\neq 0\\ 0, & \text{if } |W(t,f)|=0\end{cases}\tag{22}$$

The 2-D IF estimate $f_m(t,f)$ can be calculated as Eq. (22) for any (t,f) and for which $W(t,f)\neq 0$. When $\varphi_{k+1}'(t)-\varphi_k'(t)>4\Delta$ and $k\in\{1,\ldots,n-1\}$, two arbitrary modes are well separated with a sufficient frequency distance. Considering that the Fourier transform of the window function reaches the maximum at zero, i.e., $\widehat{g}(f)\leqslant\widehat{g}(0)$, for $t\in\mathbb{R}$; $k\in\{1,\ldots,n\}$, and then we can have:

$$f_m(t,f)=\begin{cases}\varphi_k'(t), & \text{if } f\in[\varphi_k'(t)-\Delta,\varphi_k'(t)+\Delta]\\ 0, & \text{otherwise}\end{cases}\tag{23}$$

According to the above analysis, the only post-processing method that retains the ability to perform mode recovery is to reassign the TF coefficients in the frequency direction. A novel frequency-reassignment transform named LMSSWT can be derived based on the previously proposed SSWT as follows:

$$\mathrm{LMSSWT}(t,\eta)=\int_{-\infty}^{+\infty}W(t,f)\delta(\eta-f_m(t,f))\mathrm{d}f\tag{24}$$

To prove the signal reconstruction ability of the LMSST, the following expression can be constructed:

$$\begin{aligned}\int_{-\infty}^{+\infty}\mathrm{LMSSWT}(t,\eta)\mathrm{d}\eta&=\int_{-\infty}^{+\infty}\int_{-\infty}^{+\infty}W(t,f)\delta(\eta-f_m(t,f))\mathrm{d}f\mathrm{d}\eta\\&=\int_{-\infty}^{+\infty}W(t,f)\int_{-\infty}^{+\infty}\delta(\eta-f_m(t,f))\mathrm{d}f\mathrm{d}\eta\\&=\int_{-\infty}^{+\infty}\int_{-\infty}^{+\infty}\frac{\sqrt[p]{\left[\frac{f_0(t)}{k_1}\right]^p+\left[\frac{|f_0(t)-f|}{k_2}\right]^p}}{\sqrt{2\pi}}\mathrm{e}^{-\frac{(u-t)^2}{2k^2}\left[\sqrt[p]{\left[\frac{f_0(t)}{k_1}\right]^p+\left[\frac{|f_0(t)-f|}{k_2}\right]^p}\right]^2}s(u)\mathrm{e}^{-\mathrm{i}f(u-t)}\mathrm{d}u\mathrm{d}f\\&=\int_{-\infty}^{+\infty}\int_{-\infty}^{+\infty}g_{\mathrm{w}}(u-t)s(u)\mathrm{e}^{-\mathrm{i}f(u-t)}\mathrm{d}u\mathrm{d}f\\&=2\pi\int_{-\infty}^{+\infty}g_{\mathrm{w}}(u-t)s(u)\delta(u-t)\mathrm{d}u\\&=2\pi g_{\mathrm{w}}(0)s(t)\end{aligned}\tag{25}$$

Algorithm 1 Pseudocode of LMSSWT

Step 1: Data preparation and Initialization

Initialize the seismic signal $S(t)$, and other necessary parameters. Signal length: N_t. Signal time sample interval: d_t. Discrete time length: T. Signal frequency range N_f. Frequency sample interval d_f. Parameters of TPWT: k_1 k_2 and p. Instantaneous frequency: $f_0(t)$.

Step 2: Three-parameter W transform

$0 => W(t,f)$

for $t = 1$ to N_t

for $f = 1$ to N_f

$$\frac{1}{\sqrt[p]{\left[\frac{f_0(t)}{k_1}\right]^p + \left[\frac{|f_0(t)-f|}{k_2}\right]^p}} => \sigma$$

$$\sum_{\tau=0}^{T} S(t)g(u,f,\sigma;t)\mathrm{e}^{-i2\pi f(\tau-t)} => W(t,f)$$

end for

end for

Output $W(t,f)$

Step 3: Local maximum synchrosequeezing

Calculate the IF estimate $f_m(t,f)$

$0 => LW(t,\eta)$

for $t = 1$ to N_t

for $f = 1$ to N_f

$$LW(t,\eta) + W(t,f) => LW(t,\eta)$$

end for

end for

Output $LW(t,\eta)$

Step 4: Signal reconstruction

Detect the IF trajectories $\left[t, IF_k[t]\right] k = 1,2,...,K$

for $k = 1$ to K

$$\left(2\pi g(0)\right)^{-1} \sum_{\eta \in \left[IF_k[t]-d_s, IF_k[t]+d_s\right]} LW(t,\eta) => S_k[t]$$

end for

Output $\sum_{k=1}^{K} s_k[t]$

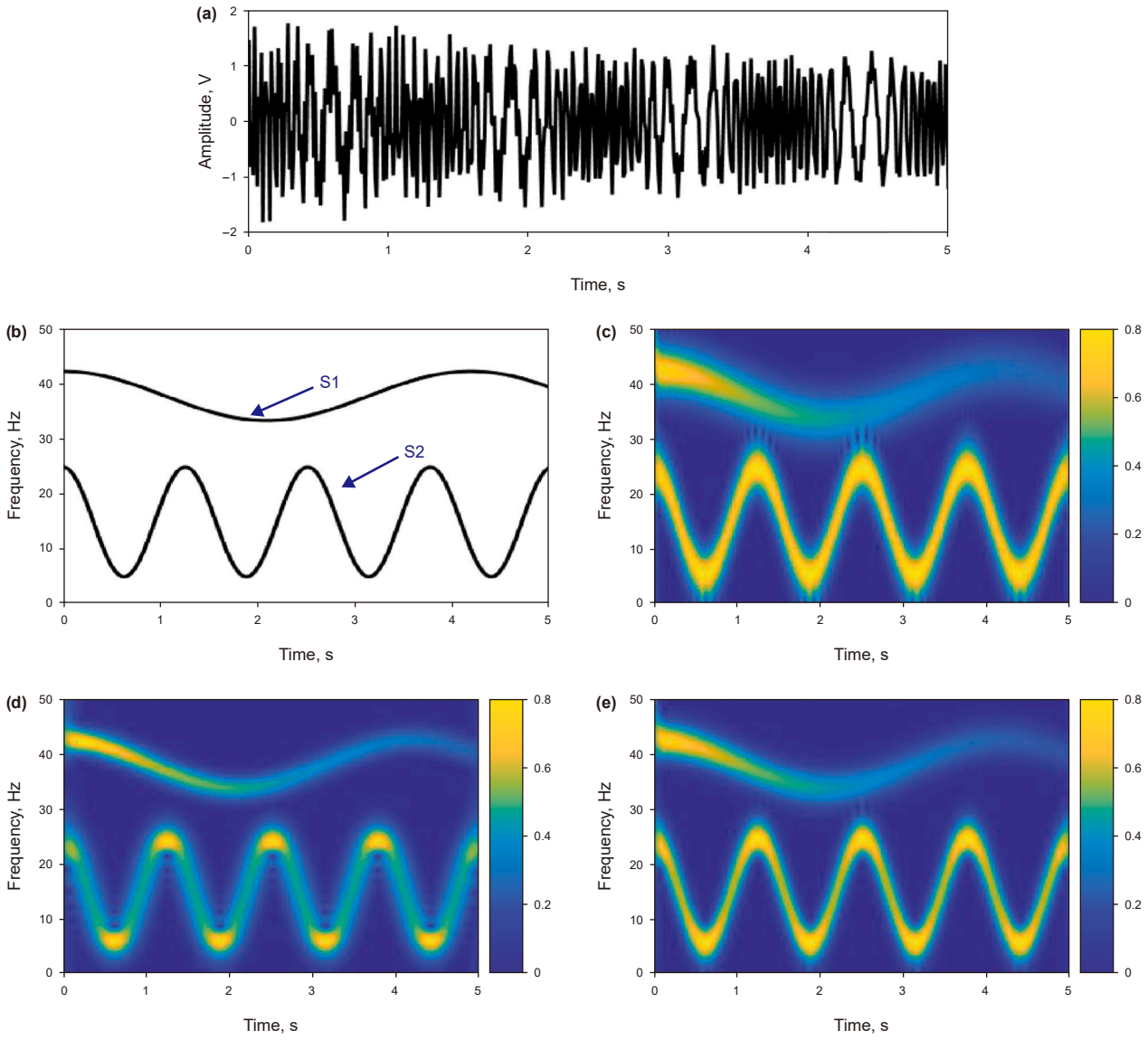

Fig. 1. **(a)** Synthetic numerical signals, **(b)** true IF trajectories, **(c)** STFT result (0.04 s), **(d)** STFT result (0.1 s), **(e)** WT result.

The original signal can be recovered by:

$$s(t) = (2\pi g_w(0))^{-1} \int_{-\infty}^{+\infty} \mathrm{LMSSWT}(t,f)\mathrm{d}f \tag{26}$$

Given that all smeared time-frequency coefficients have been reallocated to their respective instantaneous frequency (IF) regions, each mono-component mode can be reconstructed using only the coefficients located along the IF trajectories in the LMSSWT representation, expressed as:

$$s_k(t) = (2\pi g_w(0))^{-1} \mathrm{LMSSWT}\left(t, \varphi_k'(t)\right) \tag{27}$$

Prior to mode decomposition, we utilize an effective multiridge detection method to identify the instantaneous frequency (IF) trajectory of each mode (Daubechies et al., 2011; Pham and Meignen, 2017). Given the number of modes K, the IF detection is achieved by locating the local minima of the following function:

$$E(\mathrm{IF}_k(t)) = \int_{-\infty}^{+\infty} |\mathrm{TFR}(t, \mathrm{IF}_k(t))|^2 \mathrm{d}t - \int_{-\infty}^{+\infty} \left(\lambda \cdot \mathrm{IF}_k'(t)^2 + \beta \cdot \mathrm{IF}_k''(t)^2\right) \mathrm{d}t \tag{28}$$

where $(t, \mathrm{IF}_k(t))$ represents the IF trajectory estimation of the Kth mode in the TF plane, λ and β are two parameters used to adjust the level of regularization. To better understand the LMSSWT, the pseudocode is presented in Algorithm 1.

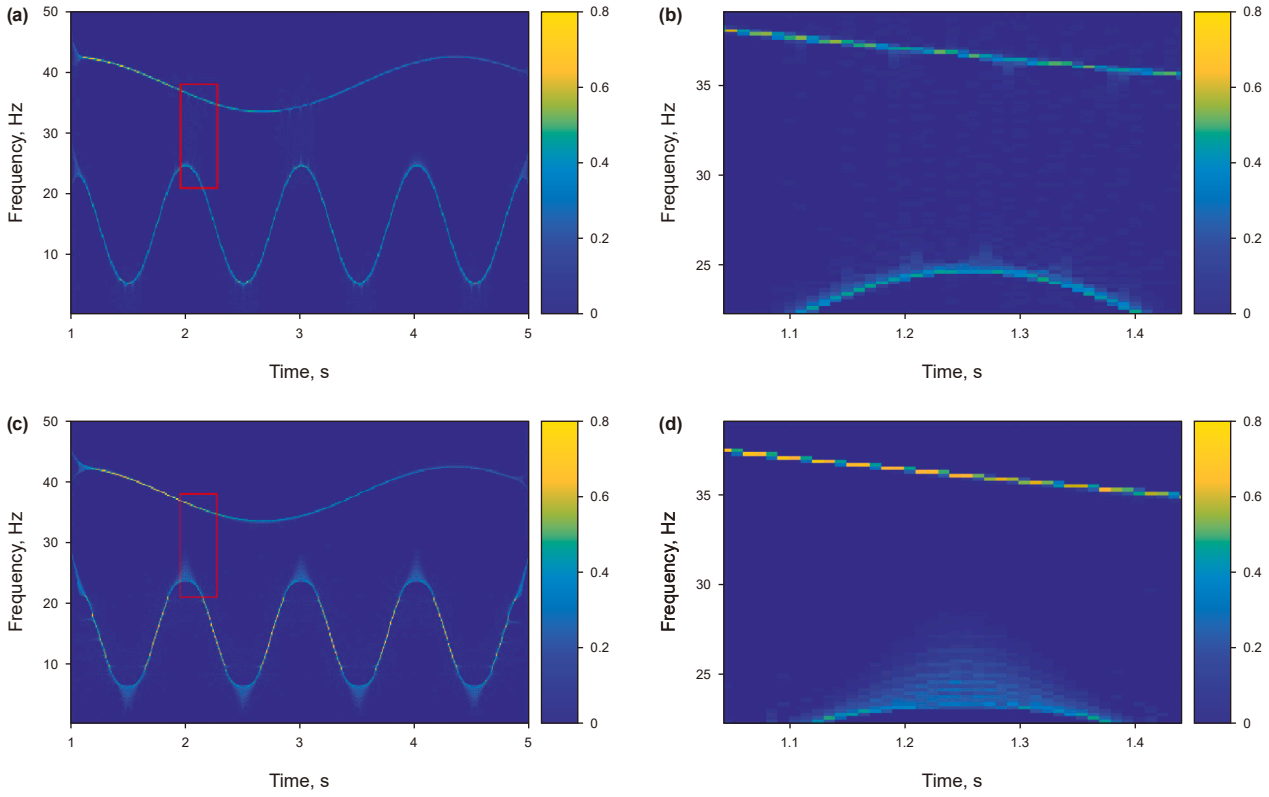

Fig. 2. **(a)** RM result (0.04 s), **(b)** zoom of RM result (0.04 s), **(c)** RM result (0.1 s), **(d)** zoom of RM result (0.1 s).

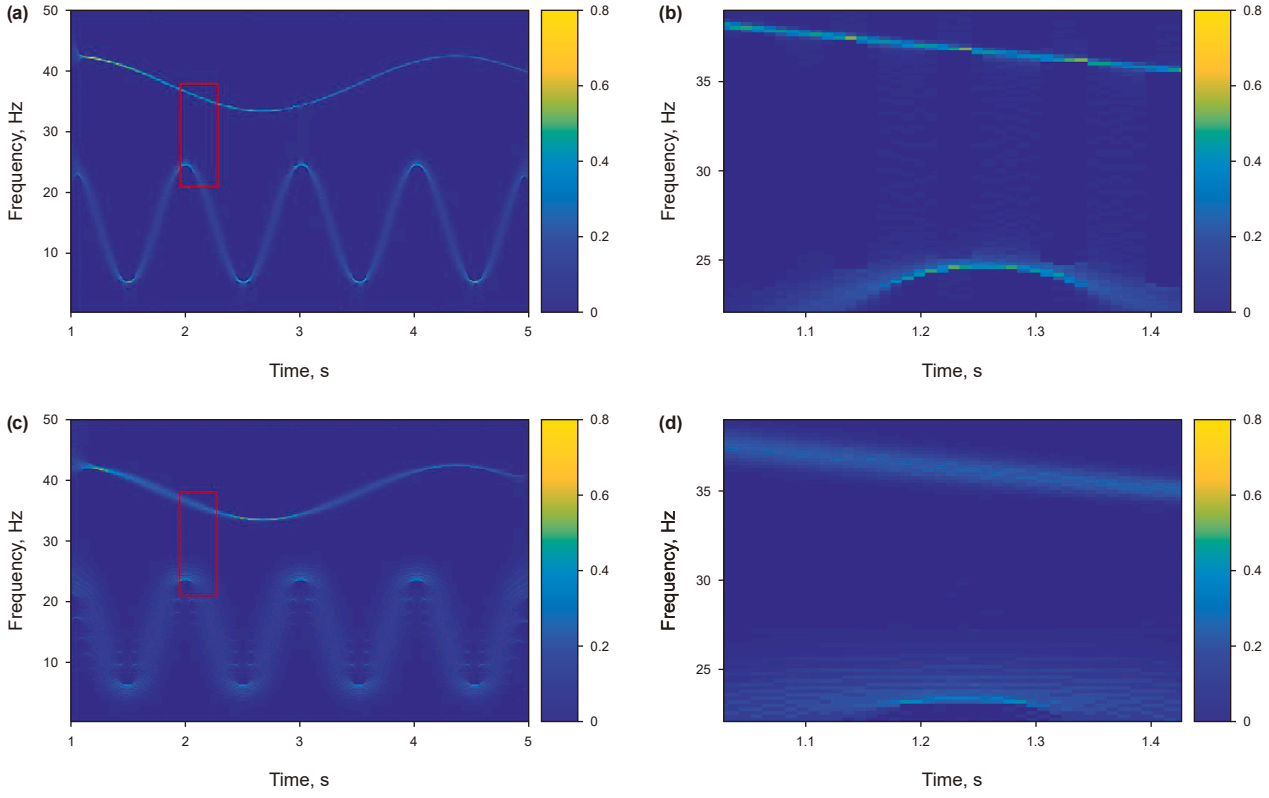

Fig. 3. **(a)** SST result (0.04 s), **(b)** zoom of SST result (0.04 s), **(c)** SST result (0.1s), **(d)** zoom of SST result (0.1 s).

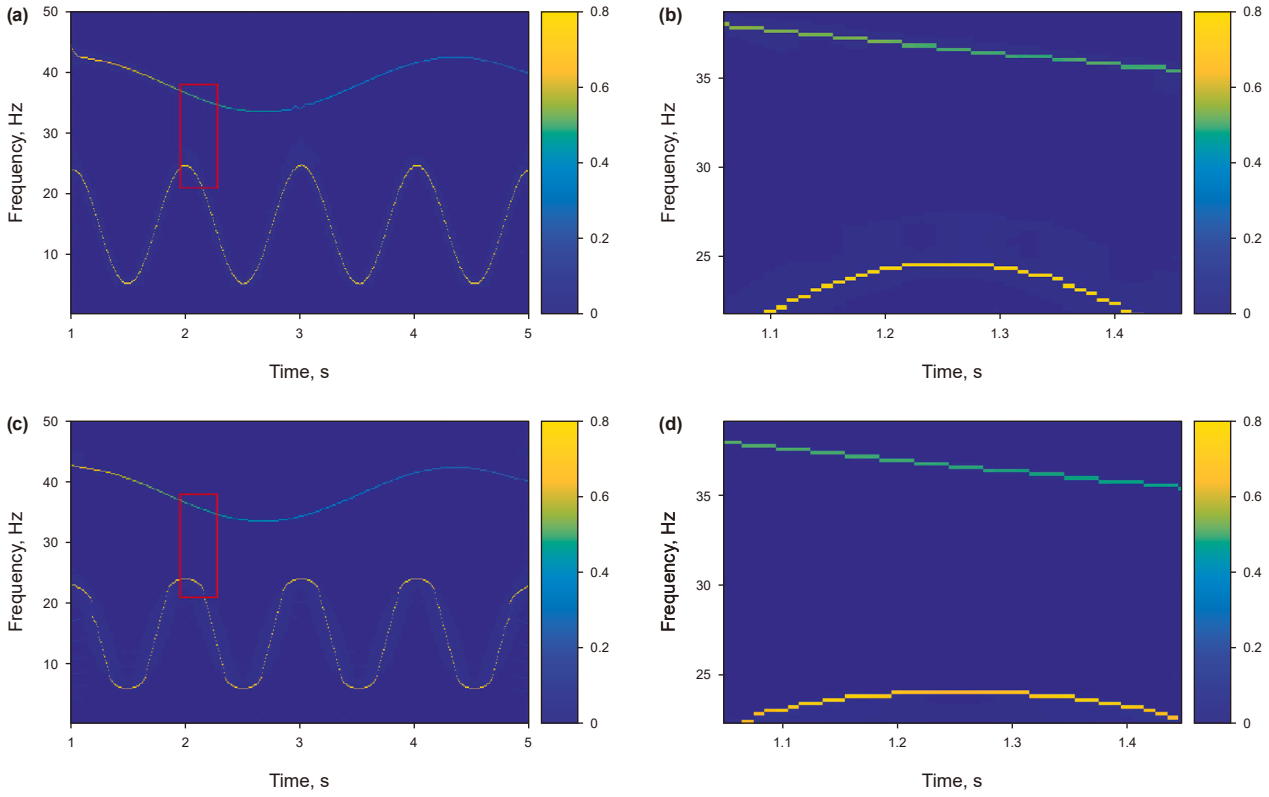

Fig. 4. **(a)** LMSST result (0.04 s), **(b)** zoom of LMSST result, **(c)** LMSST result (0.1 s), **(d)** zoom of LMSST result.

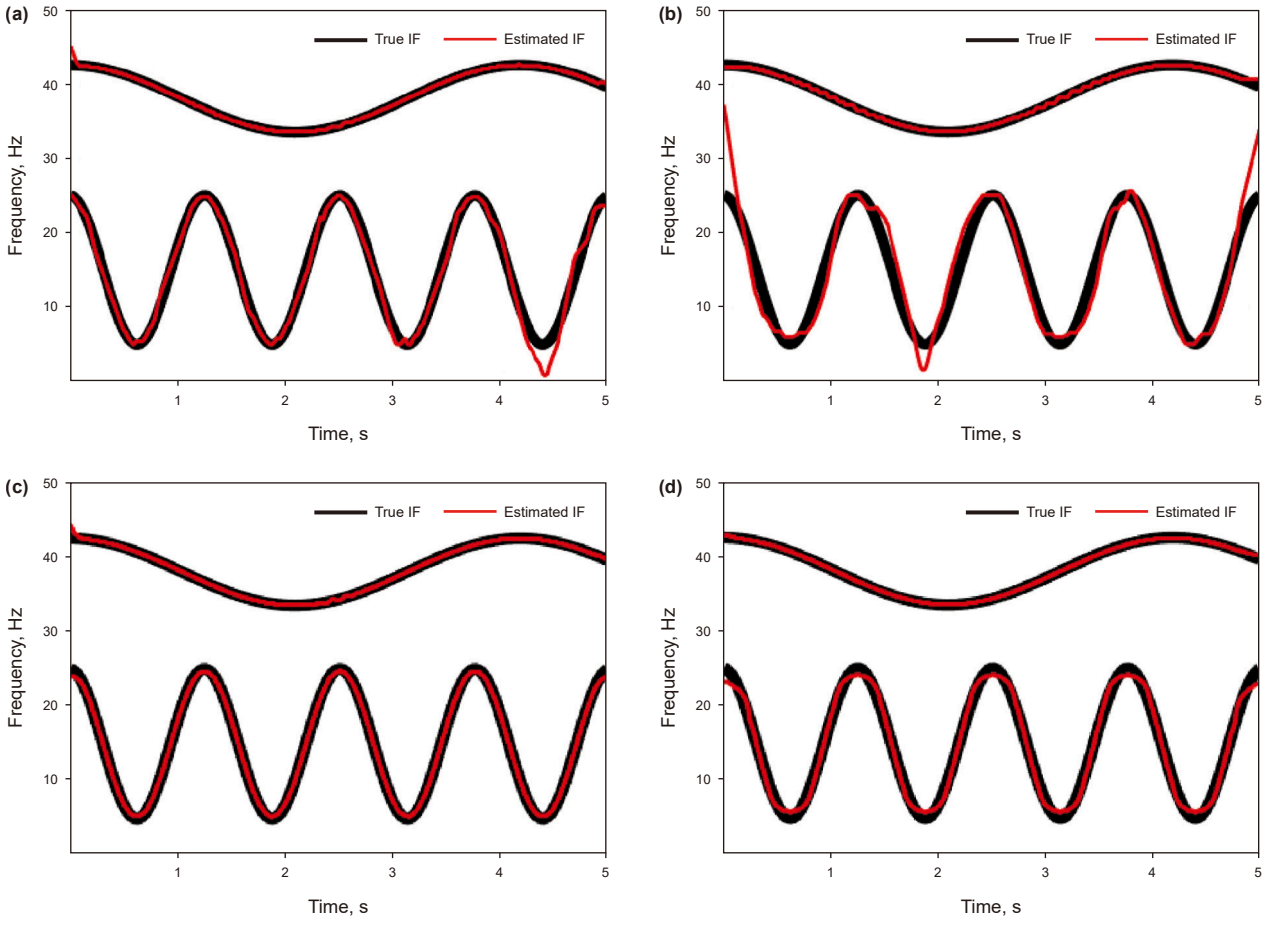

Fig. 5. **(a)** SST-based IF detection result (0.04 s), **(b)** SST-based IF detection result (0.1 s), **(c)** LMSST-based IF detection result (0.04 s), **(d)** LMSST-based IF detection result (0.1 s).

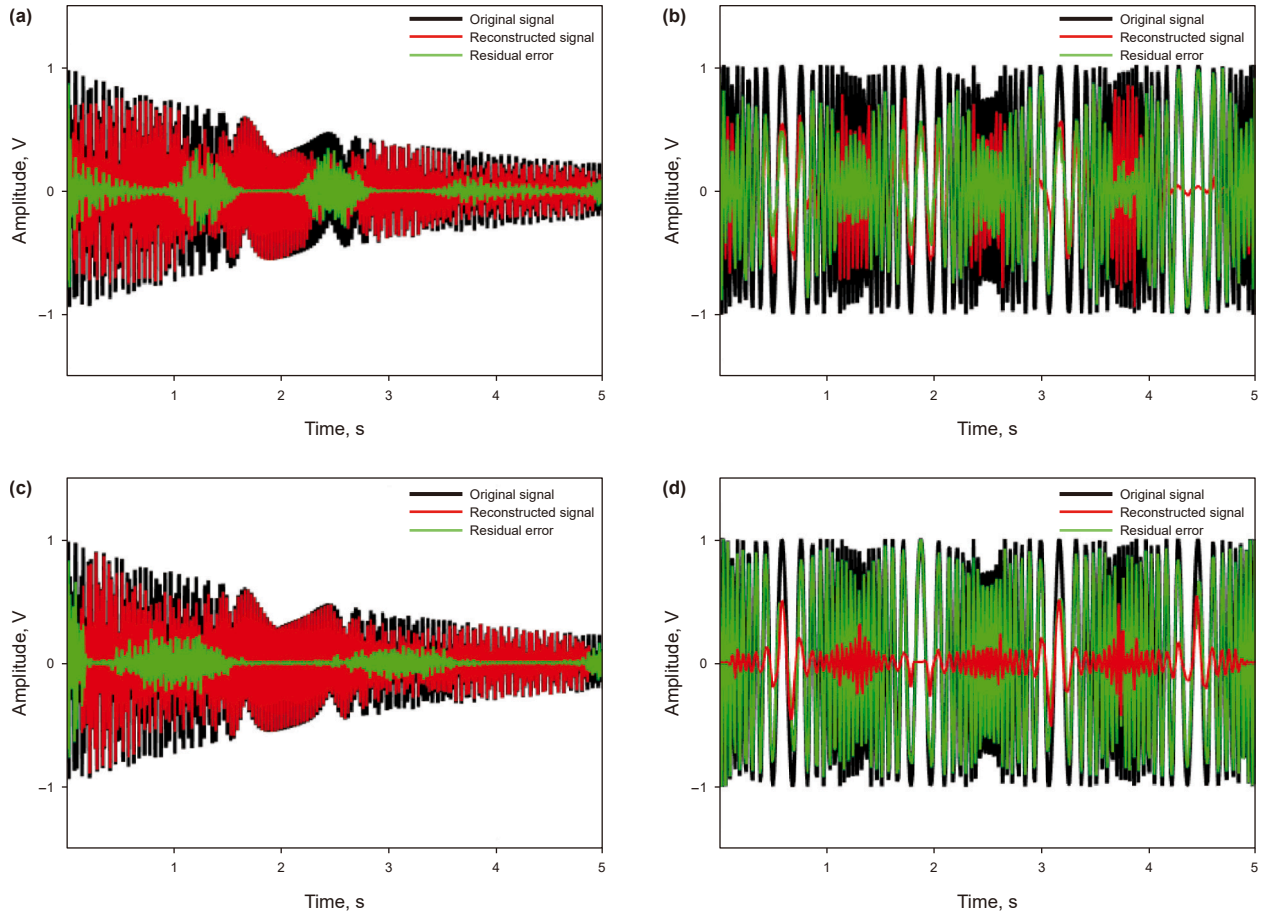

Fig. 6. **(a)** Mode S1 and **(b)** mode S2 reconstructed by SST result (0.04s), **(c)** mode S1 and **(d)** mode S2 reconstructed by SST result (0.1s).

3. Numerical experiments

To evaluate the performance of the proposed LMSSWT, we first model a multicomponent frequency-modulated (FM) signal consisting of two modes, sampled at a frequency of 100 Hz for 5 s. The signal is expressed as:

$$\begin{aligned} s(t) &= s_1(t) + s_2(t) \\ &= \mathrm{e}^{-0.3t}\sin(2\pi\cdot(38t + 3\sin(1.5t))) \\ &\quad + \sin(2\pi\cdot(15t + 2\sin(5t))) \end{aligned} \tag{29}$$

The instantaneous frequencies (IFs) of these two modes are plotted in Fig. 1(a), where it is evident that mode S2 exhibits a stronger FM law compared to mode S1. An ideal time-frequency (TF) representation should be highly concentrated along the IF trajectories. For each time point, a single frequency bin should clearly define the mono-component mode in the TF plane. Fig. 1(b) and (c) are the results of the Short-Time Fourier Transform (STFT) applied with different window lengths, which reveals poor TF resolution. The energy of the TF spectrogram smears around the IF trajectories, peaking at the IF positions but failing to accurately resolve the instantaneous frequency due to smearing. Moreover, STFT results are highly dependent on the window length, which only captures IF accurately when the window length is short. As shown in Fig. 1(d), it is obvious that the WT is unaffected by the time window length and offers greater flexibility in TF analysis. The TF results of RM and SST with the window length of 0.04 s and 0.1 s are shown in Figs. 2 and 3, which provide more concentrated representations compared to the STFT spectrogram. From the zoomed view, it is observed that RM and SST produce similarly concentrated TF results for mode S1. However, SST exhibits heavy smearing for the more rapidly varying mode S2. This denotes that RM is more suitable for characterizing the fast time-varying features than SST.

The simulated signal was processed by LMSST with the time window lengths of 0.04 s and 0.1 s, as shown in Fig. 4(a)–(d). The results display more concentrated TF features than both RM and SST. However, the RM framework is based on a spectrogram, which means that the RM cannot reconstruct the signal completely.

Further comparisons between LMSST and SST in IF detection and mode decomposition are illustrated in Fig. 5. The IF trajectories are detected from LMSST and SST results of the length 0.04 s and 0.1 s. Due to the nonlinearity of the FM signals, SST struggles to accurately reflect the FM characteristics, particularly in strongly modulated signals. The effectiveness of IF detection for both SST and LMSST depends on the window function length. Fig. 5(c) and (d) show that the detected IFs from LMSST align closely with the true IFs, highlighting the precision of LMSST in capturing IF features in strongly FM signals. In terms of mode decomposition, Figs. 6 and 7 present the two modes (S1 and S2) recovered from SST and LMSST results, respectively. The black line represents the

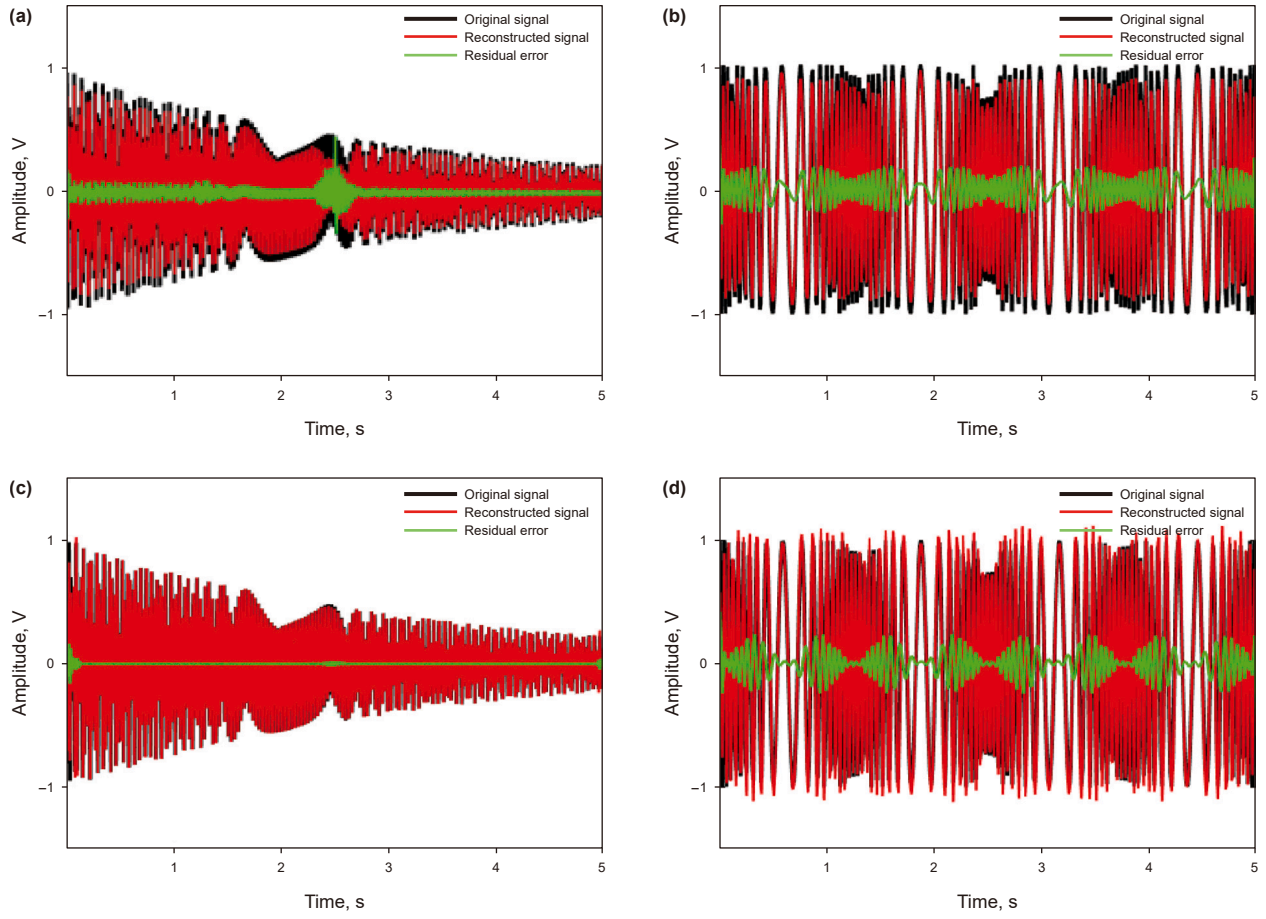

Fig. 7. **(a)** Mode S1 and **(b)** mode S2 reconstructed by LMSST result (0.04 s), **(c)** mode S1 and **(d)** mode S2 reconstructed by LMSST result (0.1 s).

original signal, the red line represents the reconstructed signal, and the green line represents the residual error. While SST roughly recovers mode S1, the recovery of mode S2 is more dependent on the window length, resulting in inconsistencies. Conversely, LMSST achieves a high approximation to the original modes for both components, and the recovery results are more stable across different window lengths. Thus, the mode decomposition accuracy of both algorithms is influenced by the length of the window function.

This modelled signal is analyzed by the proposed LMSSWT, and the results are shown in Fig. 8(a) and (b). According to the theory of LMSST, the SEO provides an effective way to detect the IF (Yu et al., 2019). The STFT and SST results have to rely on the energy of the signal itself to represent the relative time-varying features, such that the amplitude-weak modes cannot be treated fairly. The SEO result is shown in Fig. 8(c). Processed by the proposed LMSSWT, the detected IF trajectories are shown in Fig. 8(d) with high accuracy with the true IF. The mode decomposition results are listed in Fig. 8(e) and (f). The residuals of the decomposition results in Fig. 8(e) and (f) are relatively the smallest compared to the SST and STFT decomposition results, which shows that the decomposition results are highly approximated to the original time-series signals. The flexible window function enables LMSSWT can maintain high resolution without influence of the window length, setting it apart from methods that are heavily window-dependent. Since the proposed LMSSWT algorithm does not rely on the selection of the window length, its computational efficiency is higher compared to other methods. Fig. 8 clearly denotes that each mode of the signal is represented with high clarity and precision by LMSSWT, validating its effectiveness in accurately capturing and decomposing complex and nonstationary signals with strong FM characteristics.

The Rényi entropy serves as a valuable metric for assessing the energy concentration of TF representations, lower values indicating higher concentration. For a TF result $\mathrm{TFR}(t,\omega)$, the Rényi entropy H_α can be calculated as follows:

$$H_\alpha = \frac{1}{1-\alpha}\log_2 \frac{\iint \mathrm{TFR}(t,\omega)^\alpha \mathrm{d}t\mathrm{d}\omega}{\iint \mathrm{TFR}(t,\omega)\mathrm{d}t\mathrm{d}\omega} \tag{34}$$

The order α is set to 3 here. To objectively compare the TF results across different methods, Rényi entropy is calculated for each representation. In this analysis, we examine the Rényi entropies for TF representations produced by various methods of window lengths 0.04s and 0.1 s. For STFT, the Rényi entropies are 14.3632 (0.04 s) and 14.4599 (0.1 s), while the WT yields a slightly lower value of 14.1443, indicating that WT achieves a more concentrated

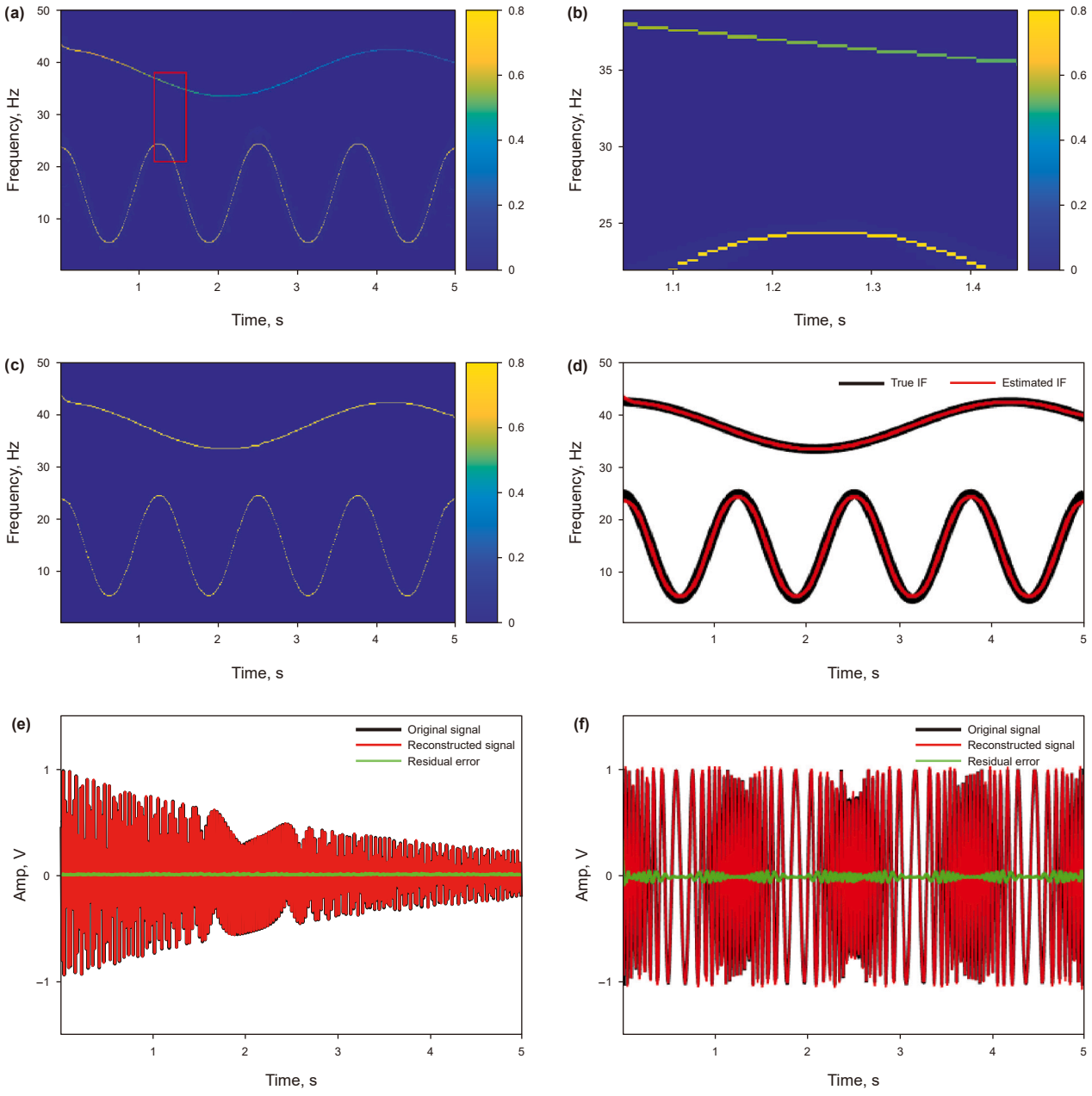

Fig. 8. (**a**) LMSSWT result, (**b**) zoom of LMSSWT result, (**c**) SEO result (0.04 s), (**d**) LMSSWT-based IF detection result, (**e**) mode S1 and (**f**) mode S2 reconstructed by LMSSWT result.

Table 1
Rényi entropy by several TFA methods of numerical signal.

TFA	STFT (0.04 s)	STFT (0.1 s)	WT	SST (0.04 s)	SST (0.1 s)
Rényi	14.3632	14.4599	14.1443	10.4778	10.6210
TFA	RM (0.04 s)	RM (0.1 s)	LMSST (0.04 s)	LMSST (0.1 s)	LMSSWT
Rényi	10.0752	10.7943	9.8001	10.3054	9.4561

TF representation than STFT. This further denotes that Rényi entropy is highly sensitive to window length, significantly impacting the TF representation concentration. SST and RM show even greater improvements, with Rényi entropies of 10.4778 (SST, 0.04 s), 10.6210 (SST, 0.1 s), 10.0752 (RM, 0.04 s), and 10.1943 (RM, 0.1 s).

The LMSST method further enhances concentration, achieving Rényi entropies of 9.8001 (0.04 s) and 10.3054 (0.1 s). The lower entropy values for LMSST reflect its effectiveness in concentrating TF energy, surpassing SST and RM. Moreover, the post-processing significantly decreases the Rényi entropy value, reflecting the importance of introducing LMSST into the WT. The LMSSWT

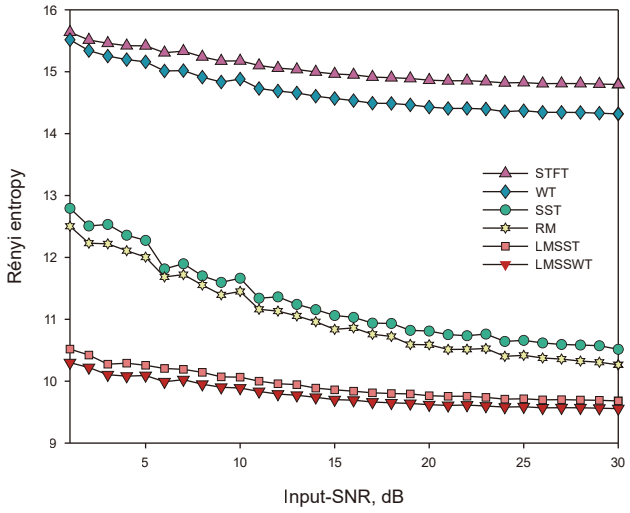

Fig. 9. Under different noise levels, the Rényi entropies of the TF results generated by six TFA methods.

achieves a Rényi entropy of 9.4561, demonstrating the most concentrated TF representation among the tested methods. As shown in Table 1, LMSSWT delivers exceptional performance in energy concentration, making it the most efficient method for representing TF features.

To test the noise robustness of LMSSWT, we add white noise to the signal while varying the signal-to-noise ratio (SNR) from 1 dB to 30 dB in Fig. 9. It can be observed that added noise increases Rényi entropy, reducing energy concentration for all methods. Among methods using a short time window (0.04 s), WT exhibits lower entropy than STFT. RM and SST yield similar entropies, lower than STFT but higher than LMSST. Importantly, LMSSWT outperforms all methods, maintaining the best TF energy concentration across different noise levels. In summary, LMSSWT not only achieves the highest energy concentration in TF representations but also has strong noise robustness, confirming its superiority in handling complex, nonstationary signals under varying noise conditions.

The second numerical signal is composed of five Ricker wavelets with different frequencies and different center times in Fig. 10(a). The central time at 0.2, 0.6, 1.0, 1.4, and 1.8 s corresponds to the Ricker wavelet whose dominant frequency is 60, 50, 40, 30, and 20 Hz, respectively. The duration of the signal is 2 s. Processed the seismic signal by different methods, and the corresponding results are presented in Fig. 10. Specifically, the time spectrum derived from the SST and RM using time windows of 0.2 s and 0.4 s is shown in Fig. 10(b)–(e). These results illustrate that both SST and RM suffer from limitations related to time window length and display poor energy concentration at higher frequencies, reducing their effectiveness for analysing nonstationary seismic signals. The short-time Fourier transform (STFT) time spectra for window lengths of 0.2 s and 0.4 s are shown in Fig. 10(f) and (h), respectively. The corresponding LMSST results are displayed in Fig. 10(g) and (i). Although LMSST provides higher resolution in both time and frequency axes, it remains constrained by window length and influenced by the limitations of STFT. Fig. 10(j) and (k) show the time spectra obtained through the W-transform (WT) and local maximum synchrosqueezing W transform (LMSSWT), respectively. The WT achieves high resolution in the time domain with strong energy concentration at both low and high frequencies. Following energy reallocation in the frequency direction, the LMSSWT displays superior resolution in both time and frequency dimensions, achieving enhanced TF energy concentration. To quantitatively evaluate the TF energy concentration of Fig. 9, we also examine the Rényi entropies for TF representations produced by various methods of window lengths 0.2 s and 0.4 s. For STFT, the Rényi entropies are 16.2806 (0.4 s) and 15.4366 (0.2 s), while the WT yields a slightly lower value of 14.7656. This indicates that the WT achieves a more concentrated time-frequency (TF) representation than the STFT. These results highlight the significant sensitivity of Rényi entropy to window length and its impact on TF concentration.

Further improvements are observed with SST and RM: SST yields entropies of 16.1388 (0.4 s) and 15.2041 (0.2 s), while RM achieves substantially lower values of 10.5249 (0.4 s) and 10.3515 (0.2 s). The LMSST method enhances concentration further, attaining entropies of 10.2821 (0.4 s) and 9.7628 (0.2 s). These lower values confirm the superior effectiveness of LMSST in concentrating TF energy compared to SST and RM. The post-processing integration of LMSST into the WT framework significantly reduces entropy, underscoring the value of this refinement. Ultimately, the LMSSWT achieves the lowest entropy of 9.1824, demonstrating the most concentrated TF representation among all tested methods. As summarized in Table 2, LMSSWT outperforms other techniques in processing nonstationary seismic signals, exhibiting superior TF aggregation and resolution.

To further evaluate the effectiveness of the LMSSWT, we apply it to a field seismic trace, shown in Fig. 11(a). The signal lasts 0.7 s with a sampling interval of 0.002 s. Fig. 11(b) and (c) illustrate the TF spectrum obtained from the STFT with window lengths of 0.04 s and 0.08 s, respectively. These spectra reveal relatively poor TF resolution, particularly in the low-frequency regions, where overlapping wavelets make it difficult to accurately pinpoint the time and center frequency of each energy group. The time spectra obtained by SST and RM of the time window length of 0.04 s and 0.08 s are shown in Fig. 11(e)–(h).

Although SST and RM provide slightly enhanced concentration compared to STFT, they struggle with resolution and display noticeable smearing in the TF plane. While LMSST offers a more concentrated TF representation with higher frequency resolution, it is still constrained by the dependency on the selected window length. This limitation affects the ability to capture time-varying features accurately, especially in low-frequency regions. The LMSSWT results in Fig. 11(k) show the advantages of combining the flexibility of WT with the energy concentration of LMSST. Each wavelet in the LMSSWT time-frequency distribution occupies a distinct time-frequency sub-region, allowing for clear separation and identification of individual wavelets. As indicated by the red arrow, LMSSWT shows superior resolution in the low-frequency regions, accurately characterizing the frequency distribution and variation of time-varying signals. This level of precision contributes significantly to understanding the dynamic characteristics of seismic signals, confirming the ability to deliver enhanced TF analysis for nonstationary seismic data.

4. 2-D examples

The complex underground structure of the overthrust model (Fig. 12(a)) is applied to verify the TF analysis characterization of

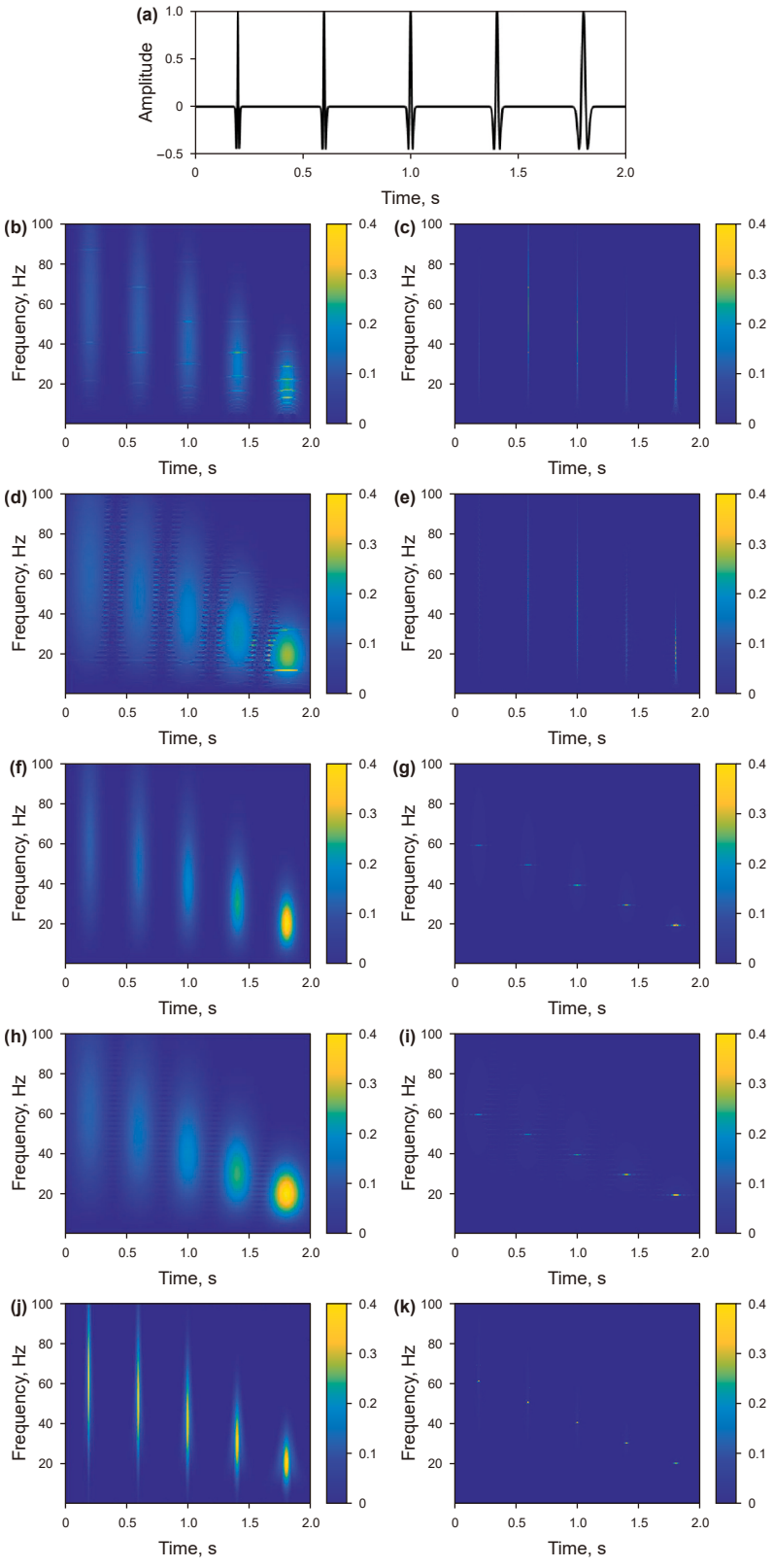

Fig. 10. Time-frequency spectra obtained by different methods for a synthetic seismic signal. **(a)** Synthetic seismic signal, **(b)** SST result (0.2 s), **(c)** RM result (0.2 s), **(d)** SST result (0.4 s), **(e)** RM result (0.4 s) **(f)** STFT result (0.2 s), **(g)** LMSST result (0.2 s), **(h)** STFT result (0.4 s), **(i)** LMSST result (0.4 s), **(j)** WT result, **(k)** LMSSWT result.

Table 2
Rényi entropy by several TFA methods of Ricker wavelets.

TFA	STFT (0.4 s)	STFT (0.2 s)	WT	SST (0.4 s)	SST (0.2 s)
Rényi	16.2806	15.4366	14.7656	16.1388	15.2041
TFA	RM (0.4 s)	RM (0.2 s)	LMSST (0.4 s)	LMSST (0.2 s)	LMSSWT
Rényi	10.5249	10.3515	10.2821	9.7628	9.1824

the proposed method. The main frequency of the wavelet of the synthetic seismic record is 20 Hz in Fig. 12(a). The data consists of 400 traces with 320 sampling points per trace, and the time sampling interval is 0.001 s. Firstly, STFT is used to process the model and extract a 20 Hz single-frequency profile, as illustrated in Fig. 12(b). The resulting profile is blurred, with indistinct stratigraphic layers that appear adhered together, making it difficult to distinguish between individual layers. In comparison, the WT improves the concentration of energy in the TF domain, providing a clearer stratigraphic profile in Fig. 12(c). The SST and RM results are presented in Fig. 12(d) and (e), respectively.

Both profiles show low values across the profile, failing to highlight the strong energy axis seen in the original model. Consequently, essential stratigraphic features are not well represented. As shown in Fig. 12(f), as a post-processing step applied to the STFT results, the LMSST sharpens the profile in the time direction, significant information is lost. The lateral continuity is compromised due to inaccuracies originating from the initial processing of STFT. On the contrary, as seen in Fig. 12(g), LMSSWT leverages the precision of the WT, resulting in a significantly clearer spectral profile. It has more obvious geological stratification, richer layer details, and better lateral continuity. The LMSSWT profile reveals well-defined layers with abundant and true stratigraphic information, even in low-frequency regions. These results underscore the effectiveness of LMSSWT in handling complex model tests, as it combines high resolution with rich stratigraphic detail, offering a robust tool for characterizing intricate underground structures.

To further validate the effectiveness of the LMSSWT, we apply it to field seismic data from East China, as shown in Fig. 13(a). This dataset consists of 451 traces with a time-migrated length of 320 samples with a sampling interval of 0.001 s. The data frequency band spans from 8 to 62 Hz. We compare the 20 Hz spectral profiles generated by STFT, WT, SST, RM, LMSST, and LMSSWT, as shown in Fig. 13(b)–(g), the spectral energy smears heavily in Fig. 13(b). Only a few seismic events are depicted, indicating the poor resolution of the STFT.

In contrast, WT yields a more energy-concentrated result (Fig. 13(c)). Almost every seismic event is displayed. Fig. 13(d) is the result of the SST. As the post-processing for the STFT result, the time direction is sharper, but most of the information is removed, and the horizontal continuity is very poor. Fig. 13(e) is the result of the RM. The inaccuracy of the STFT is responsible for this phenomenon. LMSST (Fig. 13(f)) provides an enhanced TF concentration over RM and SST, but it remains constrained by window dependency and the initial STFT limitations. Due to the precision of the WT result, the spectral profile obtained by the LMSSWT is significantly clearer in Fig. 13(g). It has more obvious geological stratification, richer layer details, and better lateral continuity.

The WT and the proposed LMSSWT have higher time and frequency resolution than other methods, and the obtained single-

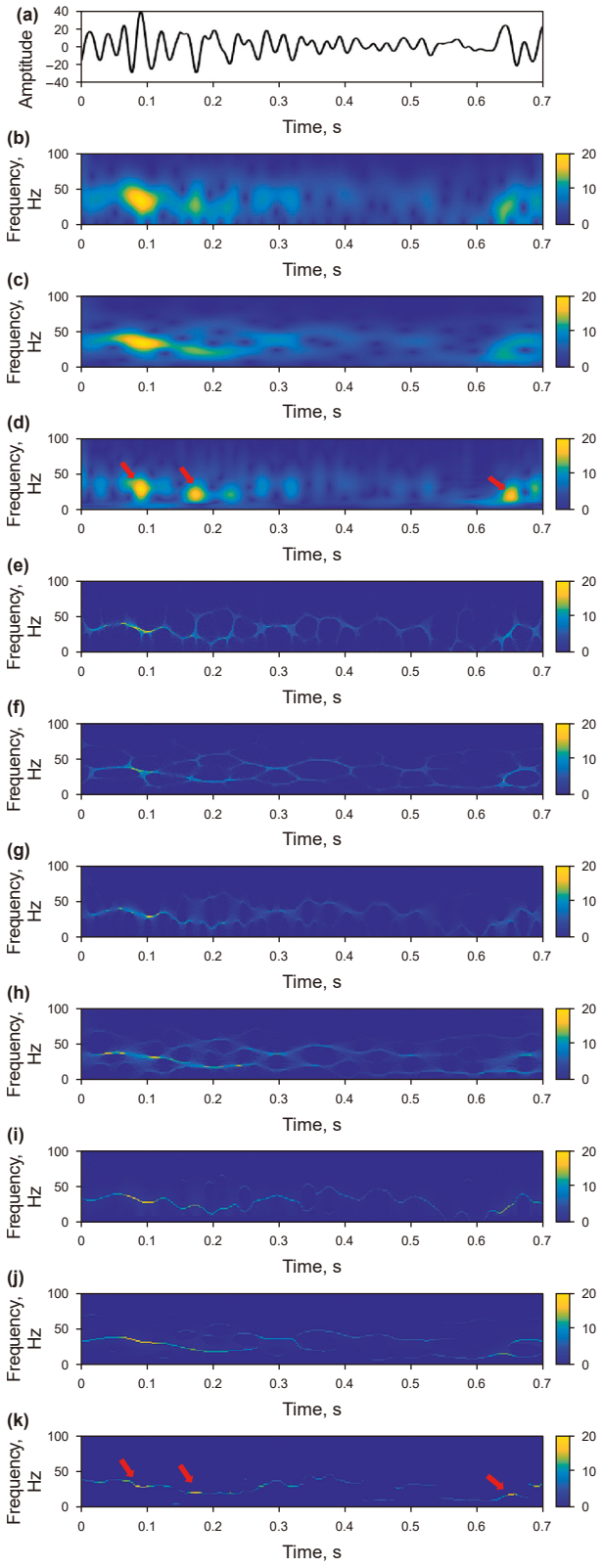

Fig. 11. Time-frequency spectra obtained by different methods for the single seismic signal. **(a)** Single seismic signal, **(b)** STFT result (0.04 s), **(c)** STFT result (0.08 s), **(d)** WT result, **(e)** SST result (0.04 s), **(f)** SST result (0.08 s), **(g)** RM result (0.04 s), **(h)** RM result (0.08 s), **(i)** LMSST result (0.04 s), **(j)** LMSST result (0.08 s), **(k)** LMSSWT result.

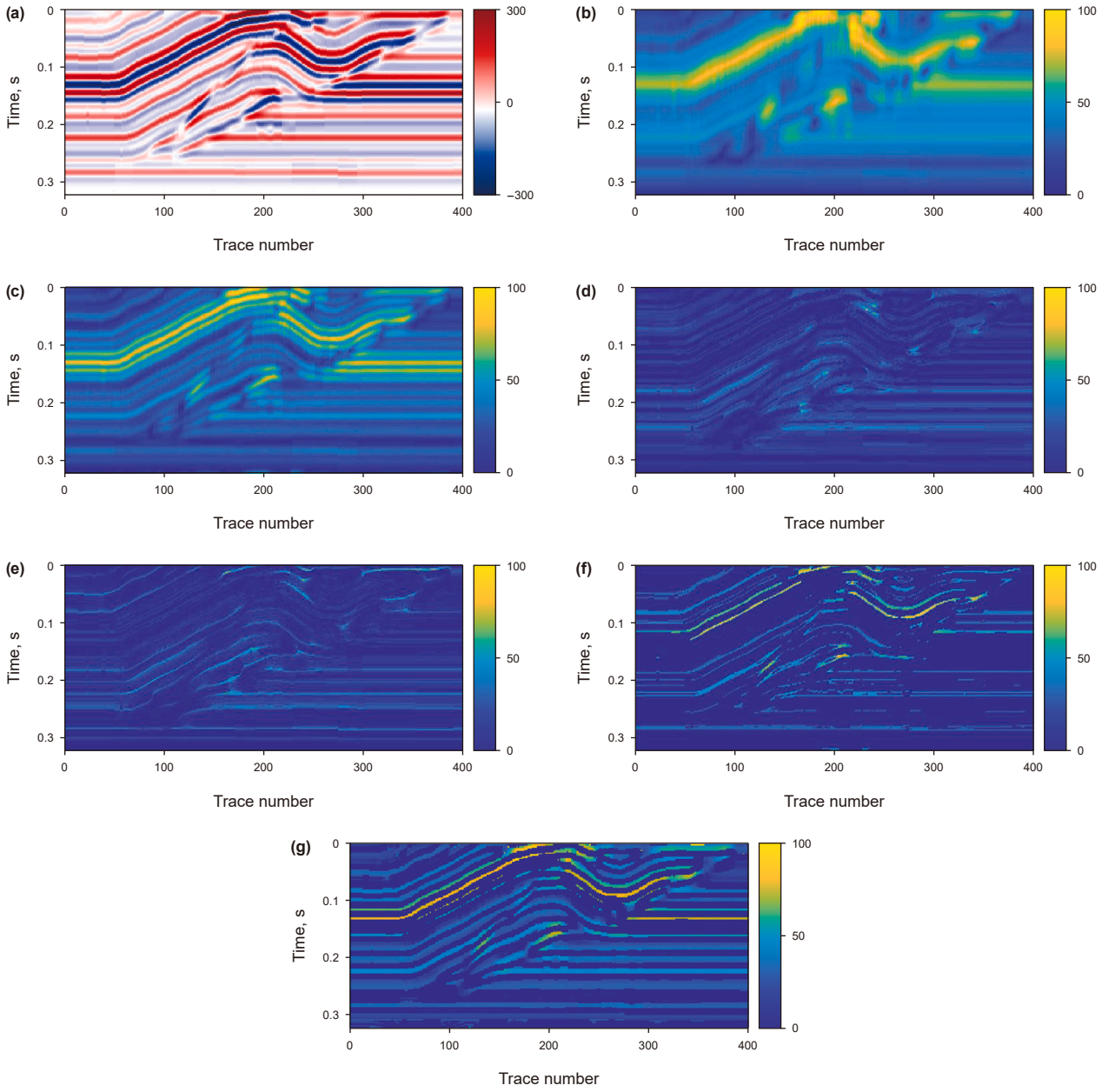

Fig. 12. 20 Hz single frequency profiles extracted by different methods. **(a)** Overthrust model, **(b)** single frequency profile generated by STFT, **(c)** single frequency profile generated by WT, **(d)** single frequency profile generated by SST, **(e)** single frequency profile generated by RM, **(f)** single frequency profile generated by LMSST, **(g)** single frequency profile generated by LMSSWT.

frequency profiles have a clear lithologic interface and obvious distinction between strong and weak energy axes. A notable advantage of the LMSSWT lies in its ability to retain effective information while eliminating false energy in single-frequency profiles, enhancing the stratigraphic and structural details in field seismic profiles. This confirms the reliability and robustness of LMSSWT in accurately capturing and representing complex subsurface structures, making it a powerful tool for seismic data analysis.

5. 3-D examples

We applied the methods to a 3D field seismic data with channels. The main sediment in the river channel is sandstone, and the other sediment is mudstone. We cut the seismic data cube to fit in the channel. The inline and crossline numbers of new data are 1332 and 480, respectively, the sampling points are 251 and the sampling interval is 0.004 s. The seismic slice by chipping along the channel formation is shown in Fig. 14(a). The reflection characteristic of sandstone in the channel is cluttered and difficult to recognize.

According to spectral decomposition theory, different underground structures have different responses to each frequency component of the incident wave, and the amplitude and phase spectra of seismic signals change during propagation due to attenuation, dispersion, and scattering. To better identify the distribution of the channel. We calculate the 20 Hz single frequency spectrum of the seismic data. The results of STFT and WT are shown in Fig. 14(b) and (c), respectively. It can be that the channel in a single frequency spectrum is more obvious than

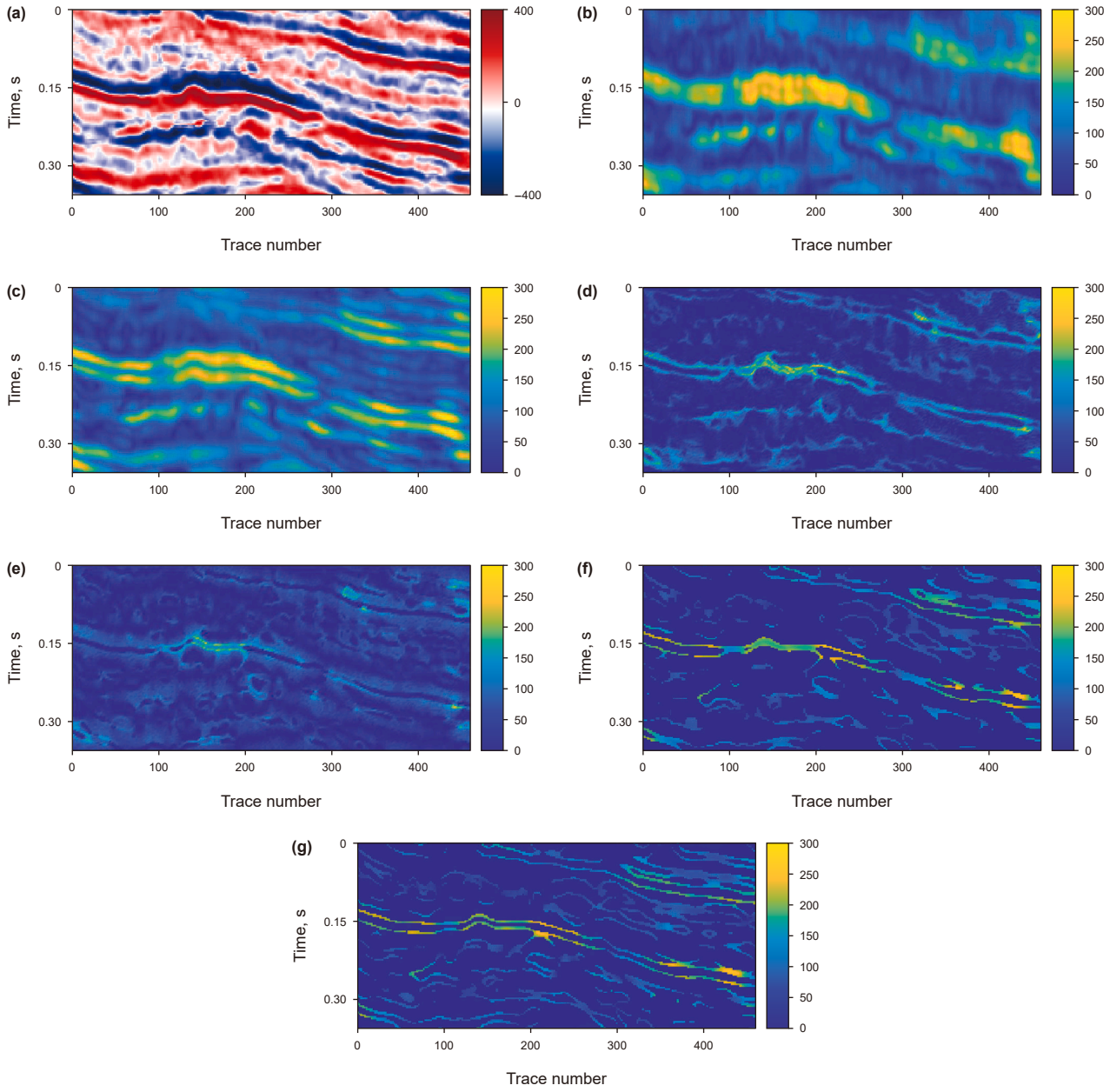

Fig. 13. 20 Hz single frequency profiles extracted by different methods. **(a)** Field seismic profile, **(b)** single frequency profile generated by STFT, **(c)** single frequency profile generated by WT, **(d)** single frequency profile generated by SST, **(e)** single frequency profile generated by RM, **(f)** single frequency profile generated by LMSST, **(g)** single frequency profile generated by LMSSWT.

seismic data. Furthermore, the channel in the WT result is clearer than the STFT result, especially in the black ellipse, which proves the WT has better resolution in low-frequency. We then use the SST, RM, LMSST and LMSSWT to identify the boundary of the channel further. RM, SST and LMSST are the post-processing of STFT results. When RM and SST remove fuzzy energy, they also remove some effective information, resulting in inaccurate results in Fig. 14(d) and (e). With less fuzzy interference, the channel in Fig. 14(f) is clearer than RM and SST, but the channel continuity is not good enough.

In contrast, the LMSSWT result in Fig. 14(g) demonstrates a clearer and more continuous edge along the channel boundary, indicating its superior resolution. Moreover, LMSSWT effectively characterizes a narrow channel that was not evident in the WT result. This outcome confirms that LMSSWT achieves higher resolution, allowing it to accurately characterize channels of varying thicknesses with clear and continuous delineation. In conclusion, LMSSWT provides high-resolution and detailed characterization of channels in the seismic data. By enhancing boundary clarity and continuity, LMSSWT produces more reliable results for seismic

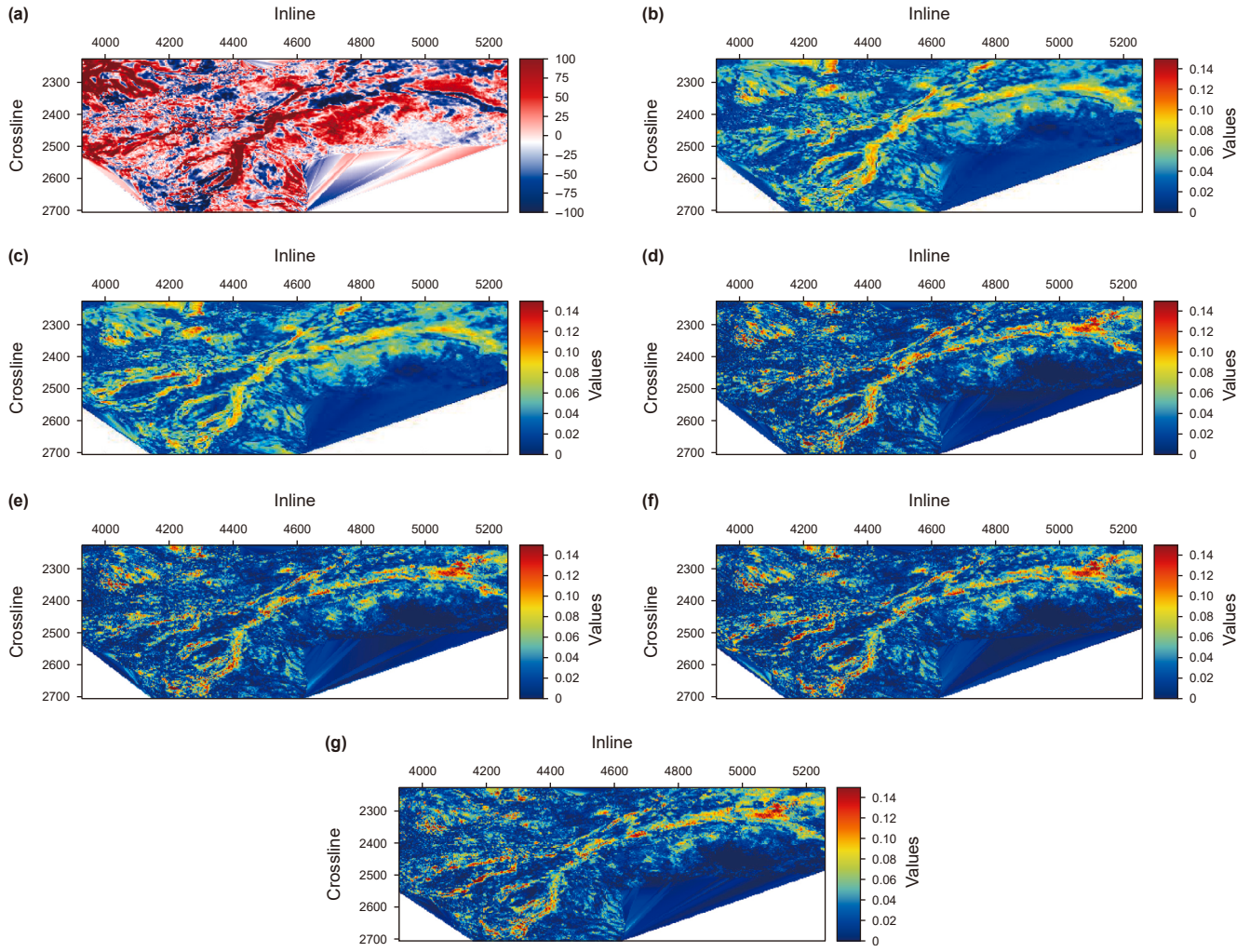

Fig. 14. Horizon slices of 3-D seismic data. **(a)** Horizon slice of seismic amplitude, **(b)** 20 Hz horizon slice generated by STFT, **(c)** 20 Hz horizon slice generated by WT, **(d)** 20 Hz horizon slice generated by SST, **(e)** 20 Hz horizon slice generated by generated by RM, **(f)** 20 Hz horizon slice generated by LMSST, **(g)** 20 Hz horizon slice generated by LMSSWT.

interpretation, making it a valuable tool for identifying and interpreting complex geological structures.

6. Conclusions

This paper proposes a novel TFA method that combines the strengths of LMSST and the W transform to achieve a more focused and centralized time-frequency representation. The development of the inverse LMSSWT further enhances its practical application, ensuring signal reconstruction and completeness. We compare the proposed method with STFT, WT, RM, SST, and LMSST in IF detection, mode decomposition and reconstruction, and anti-noise. The results show that the proposed method has a more flexible time window function and a more centralized time-frequency representation. Since the proposed LMSSWT algorithm does not rely on the selection of the window length, its computational efficiency is higher compared to other methods. The synthetic model and field data applications also validate that the proposed method can clearly characterize stratigraphic structures and accurately delineate channels of varying thicknesses, demonstrating its suitability for complex geological analysis. LMSSWT has demonstrated effectiveness in several seismic data processing, including thin layer identification and reservoir characterization. With its improved energy concentration and resolution, LMSSWT offers a promising tool for future seismic data interpretation and reservoir prediction techniques.

CRediT authorship contribution statement

Chao-He Wang: Writing – review & editing, Writing – original draft, Validation, Software, Methodology, Investigation, Formal analysis, Conceptualization. **Zhao-Yun Zong:** Writing – review & editing, Resources, Funding acquisition, Conceptualization. **Xing-Yao Yin:** Writing – original draft, Project administration, Methodology, Data curation. **Kun Li:** Visualization, Investigation. **Ying-Hao Zuo:** Validation, Software.

Declaration of interests

The authors declare that they have no known competing financial interests or personal relationships that could have appeared to influence the work reported in this paper.

Acknowledgements

The authors cordially thank the sponsorship of the National Science and Technology Major Project of China for New Oil and Gas Exploration and Development (2025ZD1402907), the National

Natural Science Foundation of China (U24B2020), and the Key Technology for Geophysical Prediction of Ultra-Deep Carbonate Reservoirs (P24240).

References

Anvari, R., Siahsar, M., Gholtashi, S., et al., 2017. Seismic random noise attenuation using synchrosqueezed wavelet transform and low-rank signal matrix approximation. IEEE Trans. Geosci. Rem. Sens. 55 (11), 6574–6581. https://doi.org/10.1109/TGRS.2017.2730228.

Auger, F., Flandrin, P., 1995. Improving the readability of time-frequency and time-scale representations by the reassignment method. IEEE Trans. Signal Process. 43 (5), 1068–1089. https://doi.org/10.1109/78.382394.

Cao, H., Xi, S.T., Chen, X.F., et al., 2016. Zoom synchrosqueezing transform and iterative demodulation: Methods with application. Mech. Syst. Signal Process. 72–73, 695–711. https://doi.org/10.1016/j.ymssp.2015.11.030.

Chen, H., Peng, L., Chen, X., et al., 2022. A three-parameter W transform and its application to gas reservoir identification. Geophysics 87 (5), V521–V532. https://doi.org/10.1190/geo2021-0803.1.

Chen, X., Chen, H., Hu, Y., et al., 2023. Statistical synchrosqueezing transform and its application to seismic thin interbed analysis. IEEE Trans. Geosci. Rem. Sens. 61, 1–13. https://doi.org/10.1109/TGRS.2023.3287334.

Chen, S., Shi, Y., Zhang, R., et al., 2024. Time sparse S-Transform (TSST) and its applications. IEEE Trans. Geosci. Rem. Sens. 62, 1–10. https://doi.org/10.1109/TGRS.2024.3420875.

Chen, X., Hu, Y., Chen, H., et al., 2025. The normalized W transform for seismic interpretation. Geophysics 90 (5), 1–63. https://doi.org/10.1190/geo2024-0678.1.

Daubechies, I., Bates, B.J., 1993. Ten lectures on wavelets. J. Acoust. Soc. Am. 93 (3), 1671. https://doi.org/10.1121/1.406784, 1671.

Daubechies, I., Lu, J., Wu, H.T., et al., 2011. Synchrosqueezed wavelet transforms: An empirical mode decomposition-like tool. Appl. Comput. Harmon. Anal. 30 (2), 243–261. https://doi.org/10.1016/j.acha.2010.08.002.

Gabor, D., 1946. Theory of communication. Part 1: the analysis of information. J. Inst. Electr. Eng.-Part III: Radio Commun. Eng. 93 (26), 429–441. https://doi.org/10.1049/ji-3-2.1946.0074.

He, Y., Jiang, Z., Hu, M., et al., 2021. Local maximum synchrosqueezing Chirplet transform: an effective tool for strongly nonstationary signals of gas turbine. IEEE Trans. Instrum. Meas. 70, 1–14. https://doi.org/10.1109/TIM.2021.3076588.

Huang, Z.L., Zhang, J.Z., Zhao, T.H., et al., 2016. Synchrosqueezing S-transform and its application in seismic spectral decomposition. IEEE Trans. Geosci. Rem. Sens. 54 (2), 817–825. https://doi.org/10.1109/TGRS.2015.2466660.

Huang, W.L., Zhou, Y.X., Zhou, Y., et al., 2024. A reweighted damped singular spectrum analysis method for robust seismic noise suppression. Pet. Sci. 21 (3), 1671–1682. https://doi.org/10.1016/j.petsci.2024.01.018.

Kakhki, M.K., Ahmadreza, M., Joaomansur, W., et al., 2022. Three-component sparse S transform. IEEE Trans. Geosci. Rem. Sens. 60, 1–7. https://doi.org/10.1109/TGRS.2022.3219420.

Lan, N.Y., Zhang, F.C., Yin, X.Y., 2022. Seismic data reconstruction based on low dimensional manifold model. Pet. Sci. 19 (2), 518–533. https://doi.org/10.1016/j.petsci.2021.10.014.

Li, Z., Gao, G., Wang, Z., et al., 2020. Time-Synchroextracting general Chirplet transform for seismic time–frequency analysis. IEEE Trans. Geosci. Rem. Sens. 58 (12), 8626–8636. https://doi.org/10.1109/TGRS.2020.2989403.

Li, R., Zhu, X., Zhou, Y., et al., 2022. Generalized W transform and its application in gas-bearing reservoir characterization. IEEE Geosci. Rem. Sens. Lett. 19, 1–5. https://doi.org/10.1109/LGRS.2021.3108836.

Li, L., Wang, Z., Yin, S., et al., 2024. Selection and application of wavelet transform in high-frequency sequence stratigraphy analysis of coarse-grained sediment in rift basin. Pet. Sci. 21 (5), 3016–3028. https://doi.org/10.1016/j.petsci.2024.06.020.

Lin, H.R., Xing, L., Li, Q.J., et al., 2022. Spatial-domain synchrosqueezing wavelet transform and its application to seismic ground roll suppression. IEEE Trans. Geosci. Rem. Sens. 60, 1–16. https://doi.org/10.1109/TGRS.2022.3210606.

Liu, N.H., Wei, S., Liu, R., et al., 2022. Seismic attenuation estimation via unscaled time–frequency representation and divergence. IEEE Trans. Geosci. Rem. Sens. 60, 1–10. https://doi.org/10.1109/TGRS.2022.3223721.

Liu, N., Lei, Y., Yang, Y., et al., 2023a. Self-supervised time-frequency representation based on generative adversarial networks. Geophysics 88 (4), 13. https://doi.org/10.1190/geo2022-0212.1.

Liu, N., Lei, Y., Liu, R., et al., 2023b. Sparse time–frequency analysis of seismic data: Sparse representation to unrolled optimization. IEEE Trans. Geosci. Rem. Sens. 61, 1–10. https://doi.org/10.1109/TGRS.2023.3300578.

Liu, N.H., Zhang, Y., Yang, Y., et al., 2024. Application of sparse S transform network with knowledge distillation in seismic attenuation delineation. Pet. Sci. 21 (4), 2345–2355. https://doi.org/10.1016/j.petsci.2024.03.002.

Luo, C., Zong, Z., 2023. The synchroextracting algorithm based on W transform and its application in channel characterization. IEEE Geosci. Rem. Sens. Lett. 20, 1–5. https://doi.org/10.1109/lgrs.2023.3262637.

Luo, C., Zong, Z., Xu, L., et al., 2022. Improved W-Transform incorporating fast matching pursuit decomposition. IEEE Geosci. Rem. Sens. Lett. 19, 1–5. https://doi.org/10.1109/LGRS.2021.3136600.

Meignen, S., Oberlin, T., Pham, D.H., et al., 2019. Synchrosqueezing transforms: From low- to high-frequency modulations and perspectives. C. R. Phys. 20 (5), 449–460. https://doi.org/10.1016/j.crhy.2019.07.001.

Pham, D.H., Meignen, S., 2017. High-order synchrosqueezing transform for multicomponent signals analysis with an application to gravitational-wave signal. IEEE Trans. Signal Process. (12), 1. https://doi.org/10.1109/TSP.2017.2686355. -1.

Sinha, S.K., Routh, P.S., Anno, P.D., et al., 2003. Time-frequency attribute of seismic data using continuous wavelet transform. In: 2003 SEG Annual Meeting,. SEG-2003-1481.

Song, Y., Le, Q., Chen, X., et al., 2023. Auto-reassigning transform for time-frequency analysis on seismic thin interbeds. IEEE Geosci. Rem. Sens. Lett. 20, 1–5. https://doi.org/10.1109/LGRS.2023.3308487.

Song, Y., Hu, Y., Chen, X., et al., 2024. Time-reassigning transform for the time–frequency analysis of seismic data. IEEE Trans. Geosci. Rem. Sens. 62, 1–11. https://doi.org/10.1109/TGRS.2024.3395902.

Stockwell, R.G., Mansinha, L., Lowe, R.P., et al., 1996. Localization of the complex spectrum: The S transform. IEEE Trans. Signal Process. 44 (4), 998–1001. https://doi.org/10.1109/78.492555.

Tian, Y., Gao, J., Wang, D., 2022. Synchrosqueezing optimal basic wavelet transform and its application on sedimentary cycle division. IEEE Trans. Geosci. Rem. Sens. 60, 1–13. https://doi.org/10.1109/TGRS.2021.3127268.

Wang, Y., 2021. The W transform. Geophysics 86 (1), V31–V39. https://doi.org/10.1190/geo2020-0316.1.

Wang, B., Lu, W., 2018. An efficient amplitude-preserving generalized S transform and its application in seismic data attenuation compensation. IEEE Trans. Geosci. Rem. Sens. 56 (2), 859–866. https://doi.org/10.1109/TGRS.2017.2755666.

Wu, Y., Huang, H., Tian, X., et al., 2024. Window parameter-optimized W-Transform method and its application. IEEE Geosci. Rem. Sens. Lett. 21, 1–5. https://doi.org/10.1109/LGRS.2024.3402747.

Xue, Y.J., Pirogova, A., Cao, J.X., et al., 2021. Q-Factor estimation by compensation of amplitude spectra in synchrosqueezed wavelet domain. IEEE Trans. Geosci. Rem. Sens. 59 (3), 2657–2665. https://doi.org/10.1109/TGRS.2020.3003122.

Yu, G., Wang, Z., Zhao, P., et al., 2019. Local maximum synchrosqueezing transform: An energy-concentrated time-frequency analysis tool. Mech. Syst. Signal Process. 117, 537–552. https://doi.org/10.1016/j.ymssp.2018.08.006.

Zhang, H.R., Liu, Y., Sun, Y.H., et al., 2024. SeisResoDiff: Seismic resolution enhancement based on a diffusion model. Pet. Sci. 21 (5), 3166–3188. https://doi.org/10.1016/j.petsci.2024.07.002.

Zhao, Z., Rao, Y., Wang, Y., 2023. The W transform with a chirp-modulated window. Geophysics 88 (2), V93–V100. https://doi.org/10.1190/geo2022-0083.1.

Zhao, Z., Rao, Y., Wang, Y., et al., 2024a. The fractional-order W-Transform. IEEE Geosci. Rem. Sens. Lett. 21, 1–5. https://doi.org/10.1109/lgrs.2023.3340161.

Zhao, Z., Rao, Y., Wang, Y., et al., 2024b. The linear canonical W-transform. Geophysics 89 (5), V469–V477. https://doi.org/10.1190/geo2023-0782.1.

Zong, Z., Fu, T., Yin, X., 2023. High-dimensional generalized orthogonal matching pursuit with singular value decomposition. IEEE Geosci. Rem. Sens. Lett. 20, 1–5. https://doi.org/10.1109/LGRS.2023.3264623.

Zong, Z., Wang, C., Luo, C., 2025. Quantification of the nonlinear effect in a seismic signal using holo-hilbert spectral analysis. Interpretation 13 (1), T87–T98. https://doi.org/10.1190/INT-2023-0063.1.